International Journal of Biological Macromolecules 246 (2023) 125632

Contents lists available at ScienceDirect

International Journal of Biological Macromolecules

journal homepage: www.elsevier.com/locate/ijbiomac

The intrinsically disordered, epigenetic factor RYBP binds to the citrullinating enzyme PADI4 in cancer cells

Salomé Araujo-Abad [a,b], María Fuentes-Baile [a,c], Bruno Rizzuti [d,e], J. Fernando Bazán [f,g], Adrián Villamarin-Ortiz [h], Miguel Saceda [a,c], Eduardo Fernández [h,i], Miguel Vidal [j], Olga Abian [e,k,l,m], Adrián Velazquez-Campoy [e,k,l,m], Camino de Juan Romero [a,c,*], José L. Neira [a,e,**]

[a] IDIBE, Universidad Miguel Hernández, 03202 Elche, Alicante, Spain
[b] Centro de Biotecnología, Universidad Nacional de Loja, Avda. Pío Jaramillo Alvarado s/n, 110111 Loja, Ecuador
[c] Unidad de Investigación, Fundación para el Fomento de la Investigación Sanitaria y Biomédica de la Comunidad Valenciana (FISABIO), Hospital General Universitario de Elche, Camí de l'Almazara 11, 03203 Elche, Alicante, Spain
[d] CNR-NANOTEC, SS Rende (CS), Department of Physics, University of Calabria, 87036 Rende, Italy
[e] Instituto de Biocomputación y Física de Sistemas Complejos (BIFI) – Unidad mixta GBsC-CSIC-BIFI, Universidad de Zaragoza, 50018 Zaragoza, Spain
[f] ħ Bioconsulting, LLC, Stillwater, MN, USA
[g] Unit for Structural Biology, Vlaams Instituut voor Biotechnologie-UGent Center for Inflammation Research, Technologiepark 71, 9052 Ghent, Belgium
[h] Instituto de Bioingeniería, Universidad Miguel Hernández, 03202 Elche, Alicante, Spain
[i] Centro de Investigación Biomédica en Red CIBER-BBN, Av. Monforte de Lemos 3-5, 28029 Madrid, Spain
[j] Centro de Investigaciones Biológicas Margarita Salas (CSIC), Calle Ramiro de Maeztu, 9, 28040 Madrid, Spain
[k] Instituto de Investigación Sanitaria Aragón (IIS Aragón), Zaragoza, Spain
[l] Centro de Investigación Biomédica en Red en el Área Temática de Enfermedades Hepáticas y Digestivas (CIBERehd), 28029 Madrid, Spain
[m] Departamento de Bioquímica y Biología Molecular y Celular, Universidad de Zaragoza, 50009 Zaragoza, Spain

ARTICLE INFO

Keywords:
Intrinsically disordered proteins
Protein-protein interactions
Fluorescence
Proximity ligation assay
Isothermal titration calorimetry
Citrullination

ABSTRACT

RYBP (Ring1 and YY 1 binding protein) is a multifunctional, intrinsically disordered protein (IDP), best described as a transcriptional regulator. It exhibits a ubiquitin-binding functionality, binds to other transcription factors, and has a key role during embryonic development. RYBP, which folds upon binding to DNA, has a Zn-finger domain at its N-terminal region. By contrast, PADI4 is a well-folded protein and it is one the human isoforms of a family of enzymes implicated in the conversion of arginine to citrulline. As both proteins intervene in signaling pathways related to cancer development and are found in the same localizations within the cell, we hypothesized they may interact. We observed their association in the nucleus and cytosol in several cancer cell lines, by using immunofluorescence (IF) and proximity ligation assays (PLAs). Binding also occurred *in vitro*, as measured by isothermal titration calorimetry (ITC) and fluorescence, with a low micromolar affinity (~1 μM). AlphaFold2-multimer (AF2) results indicate that PADI4's catalytic domain interacts with the Arg53 of RYBP docking into its active site. As RYBP sensitizes cells to PARP (Poly (ADP-ribose) polymerase) inhibitors, we applied them in combination with an enzymatic inhibitor of PADI4 observing a change in cell proliferation, and the hampering of the interaction of both proteins. This study unveils for the first time the possible citrullination

Abbreviations: AF2, AlphaFold2; ARM, armadillo; ATM, Ataxia-telangiectasia mutated protein; CD, circular dichroism; C-RING 1B, the C-terminal region of RING 1B (residues 227 to 334 of the intact protein); DAPI, 4′,6-diamidino-2-phenylindole; DED, death effector domain; DMSO, di-methyl sulfoxide; DPQ, 3,4-Dihydro-5(4-(1-piperindinyl)butoxy)-1(2H)-isoquinoline; DSB, DNA double strand break; FBS, fetal bovine serum; GBM, glioblastoma; GBSA, generalized Born surface area; IDP, intrinsically disordered protein; IF, immunofluorescence; Impα3, importin α3; ITC, isothermal titration calorimetry; MM, molecular mechanics; MTT, 3-(4,5-dimethylthiazol-2-yl)-2,5-diphenyltetrazolium bromide; NUPR1, nuclear protein 1; Pc, Polycomb; PcG, Polycomb group; PADI, protein arginine deiminase; PARP, Poly (ADP-ribose) polymerase; PBS, phosphate buffered saline; PDB, Protein Data Bank; PKP1, plakophilin 1; PRC, Polycomb Repressive Complex; PLA, proximity ligation assay; PTM, post-translational modification; RING, really interesting new gene; RYBP, RING 1A and YY 1 binding protein 1; UV, ultraviolet; YY 1, Ying and Yang 1 protein.

* Correspondence to: C. de Juan Romero, Unidad de Investigación, Fundación para el Fomento de la Investigación Sanitaria y Biomédica de la Comunidad Valenciana (FISABIO), Hospital General Universitario de Elche, Camí de l'Almazara 11, 03203 Elche, Alicante, Spain.
** Correspondence to: J.L. Neira, IDIBE, Edificio Torregaitán, Universidad Miguel Hernández, Avda. del Ferrocarril s/n, 03202 Elche, Alicante, Spain.
E-mail addresses: m.juan@umh.es (C. de Juan Romero), jlneira@umh.es (J.L. Neira).

https://doi.org/10.1016/j.ijbiomac.2023.125632
Received 5 April 2023; Received in revised form 16 June 2023; Accepted 28 June 2023
Available online 2 July 2023

of an IDP, and suggests that this new interaction, whether it involves or not citrullination of RYBP, might have implications in cancer development and progression.

1. Introduction

RYBP (Ring1A and YY 1 binding protein, UniProt number Q8N488) was first characterized as an interacting partner of the Polycomb group (PcG) protein Ring1A [1] and a non-canonical component of the Polycomb Repressive Complex 1 (PRC1) [2,3–5]. RYBP is a pro-apoptotic protein, whose apoptosis regulation can occur through: (i) the modulation of the necrosis factor alpha receptor family modulation; (ii) the stabilization of p53; or (iii) the direct interaction with death effector domain (DED)-containing proteins [2,6,7,8,9]. RYBP binds to the E3-ubiquitin ligase MDM2 to inhibit the MDM2-mediated p53 ubiquitylation, thus, stabilizing and increasing p53 activity [10]. Therefore, RYBP can be seen as a regulator of the p53-MDM2 loop, and it can be considered as a tumor suppressor. However, depending on the cancer type, it has been observed that RYBP can work as a tumor suppressor gene or, alternatively, as an oncogene [2,6]. From a functional point of view, RYBP is a ubiquitin-binding-domain-containing protein and binds to ubiquitylated proteins [2,11–13]. During transcriptional control, RYBP also interacts with DNA-binding proteins, such as the members of the E2F family of transcription factors, among others, and with YY 1 [14]. In this regard, RYBP appears to be another multi-tasking protein with the ability to participate in several events and routes. From a structural point of view, RYBP is a 228-residue-long, highly basic IDP, which binds to DNA [2,15], and it folds upon interacting with it. As other IDPs, RYBP does not have a unique stable conformation, resulting in a high structural flexibility, easing its interaction with several macromolecules allowing the functions described above [16–19]. It contains a nuclear location signal which allows nuclear translocation through the nuclear pore, and therefore, to carry out its transcriptional function [20]. In its N-terminal region, there is a C2-C2 Zn finger domain, which contains the ubiquitin-binding function [12,21].

RYBP is actively removed from DNA damage sites due to its ability to bind to K63-ubiquitin chains at sites of double strand breaks (DSBs) [22]. This probably leads to the fact that RYBP overexpression sensitizes cancer cells to DNA damaging agents [22,23]. Moreover, it has been recently shown that RYBP sensitizes several cancer cell lines to Poly-(ADP-ribose)-polymerase (PARP) inhibitors by regulating ataxia-telangiectasia mutated protein (ATM) activity [24]. ATM is a protein kinase that is early activated in response to DNA damage [25,26]. ATM is present as an inactive dimer that later monomerizes in the presence of DSBs [27]. ATM activation results in a cascade of phosphorylation reactions beginning with its autophosphorylation that decondenses chromatin at DNA damage sites to increase the accessibility for DNA repair proteins, and leads to the phosphorylation of numerous downstream targets [27].

PARP is a crucial enzyme in base excision mending and single strand break repair pathways, as it binds to DNA end at both DSBs and single strand ones for reparation [28,29]. Inhibition of PARP blocks the repairs of DNA strand breaks and sensitizes cancer cells to various DNA damaging agents [25]. Therefore, the loss of PARP activity results in an increase in the number of damaged DNA sites repaired by homologous recombination. For these reasons, PARP inhibitors have been broadly used as anticancer treatments, being particularly efficient in the tumor context of inhibited homologous recombination DNA repair mechanisms. So far, four PARP inhibitors (olaparib, niraparib, rucaparib, and veliparib) have been approved by the FDA for clinical use. However, PARP inhibitors were originally developed to sensitize tumors to agents that cause tumor damage, including ionizing radiation, alkylating agents such as temozolomide, and topoisomerase I inhibitors such as camptothecin [30–33].

PADI4 is a member of a family of peptidyl-arginine deiminases (PADI4, UniProt number Q9UM07), capable of catalyzing citrullination, *i.e.*, the conversion of arginine to citrulline residues in a polypeptide, in the presence of Ca(II). This post-translational modification (PTM) affects the molecular properties of the polypeptide chain [34,35,36,37]. There are five human genes encoding PADI proteins, appropriately named: PADI1-6 [38–43]. The majority are dimers, with monomers having 663 to 694 residues. Each *PADI* gene has a different pattern of expression depending on the tissue, cell type, cell differentiation stage and physiological or pathological conditions; these conditions result in a specific localization of the isozyme expressed. In particular, PADI4 is located in cytoplasmic granules of inflammatory cells (eosinophils, neutrophils and macrophages), mammary gland cells, stem cells, and tumor cells, where it is highly expressed, either in the cytosol or in the nucleus. PADI4 is involved in gene transcription and immune system modulation [44–46,47,48]. Furthermore, PADI4 is involved in p53-gene expression, as well as in the expression of other p53-target genes [48–50]. We have shown recently that PADI4 is expressed in glioblastoma (GBM), pancreatic adenocarcinoma, and colon cancer [51]. Moreover, PADI4 binds to other key proteins involved in cancer development, such as importin α3 (Impα3) [52], plakophilin 1 (PKP1) [53], and nuclear protein 1 (NUPR1) [54], another IDP.

It has been also shown that RYBP and NUPR1 interact with the C-terminal region of RING 1B, a member of PRC1 [55]; both proteins are transcription factors and they are involved in protein routes related to p53 [56–59]. As it happens with NUPR1, RYBP has a highly basic isoelectric point, which is complementary to that of PADI4. Based on these data, we hypothesized that RYBP could also interact with PADI4, and this could shed some light into the mechanisms of tumorigenesis. In this work, we identified and characterized the interaction between RYBP and PADI4 *in cellulo* by means of immunofluorescence (IF) and proximity ligation assay (PLA) in several cancer cell lines. Furthermore, *in vitro* studies by using a combination of biophysical techniques including fluorescence, far-ultraviolet (UV) circular dichroism (CD) and ITC, as well as molecular modeling supported the binding between both proteins. The interaction occurred with a dissociation constant in the low micromolar range, as measured by ITC ($K_d \sim 1$ μM) and fluorescence ($K_d \sim 10$ μM). Structure prediction and molecular modeling studies indicated that the PADI4-binding region of RYBP corresponded to residues G^{49}TSTRKPR^{56}, with residue Arg53 directed engaged in the active site of the PADI4. PLAs in the presence of GSK484, an enzymatic inhibitor of PADI4, hampered the binding of both proteins. Thus, our *in cellulo* and *in silico* results suggested that RYBP could be a new substrate of the citrullinating enzyme PADI4. However, the hampering of such interaction in the presence of PADI4 inhibitors could be due also to allosteric effects in the protein. Furthermore, proliferation studies in the presence of 3,4-Dihydro-5(4-(1-piperindinyl)butoxy)-1(2H)-isoquinoline (DPQ), a PARP inhibitor, and GSK484 indicated a synergistic effect in tumor suppression on pancreatic tumor cells. Taken together our findings indicate that the hampering of the interaction between PADI4 and RYBP might have key applications in the therapeutic suppression and development of some tumors.

2. Materials and methods

2.1. Materials

Imidazole, Trizma base, DNase, SIGMAFAST protease tablets, NaCl, Ni^{2+}-resin, DAPI (4′,6-diamidino-2-phenylindole), 3-(4,5-dimethylthiazol-2-yl)-2,5-diphenyltetrazolium bromide (MTT), di-methyl sulfoxide (DMSO), GSK484 and Amicon centrifugal devices with a molecular weight cut-off of 3 and 30 kDa were from Sigma-Merck (Madrid, Spain).

The β-mercaptoethanol was from BioRad (Madrid, Spain). Ampicillin and isopropyl-β-D-1-thiogalactopyranoside were obtained from Apollo Scientific (Stockport, UK). The DPQ was from Calbiochem (San Diego, CA, USA). Triton X-100, Tris(2-carboxyethyl)phosphine (TCEP), the dialysis tubing with a molecular weight cut-off of 3500 Da and the SDS protein marker (PAGEmark Tricolor) were from VWR (Barcelona, Spain). The rest of the materials were of analytical grade. Water was deionized and purified on a Millipore system.

2.2. Protein expression and purification

PADI4 and RYBP were purified by His-tag affinity chromatography, as previously described [15,51]. Briefly, PADI4 was in a codon-optimized, vector pHTP1 (kanamycin resistant) and with an N-terminal His-tag. The vector was synthesized and produced by NZytech (Lisbon, Portugal). Expression of PADI4 was carried out in *E. coli* BL21 (DE3) strain (Merck, Madrid, Spain). The protein was expressed with a final amount of 0.8 mM of IPTG, when the absorbance units at 600 nm of 1 L of LB medium reached a value in the range 0.8-1.0. After induction, cells were grown overnight at 30 °C. The His-tag of PADI4 was kept in all experiments. On the other hand, RYBP was cloned in an in-house modified version of a pQE30 vector, with a His-tag at the N-terminus. The expression vector used had an additional six-His tag at the N-terminus, which does not contain any cleavage site. Expression was carried out in *E. coli* BL21 (DE3) strain. The protein was expressed with a final amount of 1 mM of IPTG, when the absorbance units at 600 nm of 1 L of LB medium reached a value in the range 0.8-1.0. After induction, cells were grown at 37 °C for 16 h.

In all cases, protein concentrations were determined by UV absorbance, employing an extinction coefficient at 280 nm estimated from the number of tyrosines and tryptophans in each of these proteins [60]. The PADI4 construct has ten tryptophans and thirteen tyrosines *per* monomer, and that of RYBP has one tryptophan and one tyrosine.

2.3. Cell lines

Isolation of the primary human GBM cell lines HGUE-GB-42 was performed from surgical washes, as reported previously [61]. Human pancreatic adenocarcinoma (RWP-1) and colorectal cancer (SW-480) cell lines were donated by Instituto Municipal de Investigaciones Médicas (IMIM, Barcelona, Spain) [62]. The RWP-1 and SW-480 cell lines were cultured in Dulbecco's Modified Eagle's Medium: High Glucose (DEMEM-HG) (Biowest, MO, USA). Cells were cultured in Dulbecco's Modified Eagle's Medium: Nutrient Mixture F-12 (DMEM F-12) (Biowest, MO, USA), supplemented with 10 % (*v*/v) heat-inactivated fetal bovine serum (FBS) (Capricorn Scientific, Ebsdorfergrund, Germany) and 1 % (v/v) penicillin/streptomycin mixture (Biowest, MO, USA). Cells were incubated at 37 °C in a humidified 5 % CO_2 atmosphere as previously described [61,63].

2.4. Immunofluorescence (IF)

An amount of 30,000 cells of HGUE-GB-42, SW-480, and RWP-1 cell lines were seeded into twenty-four-well plates on coverslips. After 24 h, they were fixed with paraformaldehyde at 4 % concentration and blocked with FBS/PBS (phosphate buffered saline) (1 ×) (50 μL/mL). Next, cells were incubated with anti-PADI4 (1:200, mouse; Abcam, Cambridge, UK) and anti-RYBP (1:100, home-made) antibody [1]. After washing out the first antibody, cells were incubated with Alexa Fluor 568-labeled anti-mouse (1:500) and Alexa Fluor 488-labeled anti-rabbit (1:500) secondary antibodies (Invitrogen, Barcelona, Spain); the DAPI (4′,6-diamidino-2-phenylindole) reagent was used to stain the nucleus. Coverslips were mounted in Prolong™ Gold Antifade Reagent (Invitrogen, Barcelona, Spain) and analyzed using an Axio Observer Z1 inverted microscope (Carl Zeiss, Oberkochen, Germany) at × 63 magnification.

2.5. Proximity ligation assay (PLA)

An amount of 30,000 cells of HGUE-GB-42, SW480 and RWP-1 cell lines were seeded in twenty-four-well plates on coverslips. After 24 h, cells were washed twice in PBS (1 ×), fixed, washed twice again, permeabilized in PBS, with 0.2 % Triton X-100, and saturated with blocking solution for 30 min before immune-staining with Duolink by using PLA Technology (Merck, Madrid, Spain), following the manufacturer's protocol. Anti-PADI4 primary antibody was used. Then, slides were processed for *in situ* PLA by using sequentially the Duolink *In Situ* Detection Reagents Red, Duolink *In Situ* PLA Probe Anti-Mouse MINUS, and Duolink *In Situ* PLA Probe Anti-Rabbit PLUS (Merck, Madrid, Spain). In these experiments, red fluorescence signal corresponds to the PLA-positive signal, and it indicates that the two proteins are bound, forming a protein complex; on the other hand, blue fluorescence signal corresponds to nuclei (DAPI staining). Both negative and positive control experiments, the former by omitting one of the primary antibodies, were performed. Image acquisition was carried out by using a confocal LSM900 with Airyscan 2 microscope (Carl Zeiss, Oberkochen, Germany) at × 63 magnification. We used a customized protocol that enables the quantification of interactions detected by PLA by using the public domain image processing program ImageJ (Fiji, Hamamatsu, Japan) software. Confocal images were processed until a binary image with only two-pixel intensities, black and white, was created. We adjusted the parameters for nuclear or cytoplasmic analysis by using DAPI to outline the nucleus of the cell. An image of the nuclei included in the analysis was generated together with a summary table of the number of selected nuclei.

In experiments with PADI4 inhibitor, cells were previously subjected to a treatment with GSK484 at 20 μM concentration for 24 h, while the control cells remained untreated for the same period of time, since the drug was dissolved in water. After that, PLA experiments were performed.

2.6. Proliferation assay

The antiproliferative capacity of GSK484, in isolation, was explored in the concentration range 1-4 μM. Monotherapy of DPQ, a PARP inhibitor, was performed in a concentration range from 1 to 15 μM. The proliferation assays of both isolated compounds and their cocktails were analyzed by using a colorimetric assay, based on the reduction reaction catalyzed by the mitochondrial enzyme succinate dehydrogenase. Then, after addition of the yellow-colored MTT compound, the succinate dehydrogenase in viable cells catalyzes the opening of its tetrazolium ring, generating purple formazan salts ((E,Z)-5-(4,5-dimethylthiazol-2-yl)-1,3-diphenylformazan), which are insoluble and impermeable to the plasma membrane.

Initially, RWP-1 cells were seeded in 96-well plates at a density of 3000-4000 cells *per* well depending on the size and growth rate of the cell line. After 24 h, the corresponding treatments (namely, isolated GSK484, isolated DPQ, or the cocktails containing both) were added in quadruplicate; cells were kept in culture for 72 h. At the end of the treatment time, MTT was added at a final concentration of 0.25 mg/mL for 3 h. During the whole time of the assay, the cells were kept in an incubator at 37 °C with 5 % CO_2. Next, the contents of the wells were removed and 200 μL of DMSO were added; the plates were kept 30 min, at room temperature and under intense agitation to dissolve the formazan crystals. Finally, the absorbance of the plates was measured at 570 nm on a Gen5™ plate reader (BioTeK®, Winooski, VT, United States).

For the treatment by using the cocktails of DPQ and GSK484, first we maintained a constant GSK484 concentration of 4 μM, while that of DPQ was varied from 5 to 15 μM. In the other cocktail treatment, the concentration of DPQ was kept constant at 15 μM, and that of GSK484 was changed from 1 to 4 μM.

2.7. Fluorescence

2.7.1. Steady-state fluorescence

Fluorescence spectra were collected on a Cary Eclipse Varian spectrofluorometer (Agilent, Santa Clara, CA, USA), interfaced with a Peltier unit. Following the standard protocols used in our laboratories, the samples were prepared the day before and left overnight at 5 °C; before experiments, samples were left for 1 h at 25 °C. A 1-cm-pathlength quartz cell (Hellma, Kruibeke, Belgium) was used. Concentration of PADI4 was 3 μM (in protomer units), and that of RYBP was 20 μM. Experiments were performed in 20 mM Tris buffer (pH 7.5), 5 mM TCEP, 150 mM NaCl and 5 % glycerol. Protein samples were excited at 280 and 295 nm. The other experimental parameters have been described elsewhere [64]. Appropriate blank corrections were made in all spectra. Fluorescence experiments were repeated in triplicates with newly prepared samples. Variations of results among the experiments were lower than 5 %.

2.7.2. Binding experiments with PADI4

For the titration between RYBP and PADI4, increasing amounts of RYBP, in the concentration range 0-20 μM, were added to a solution with a fixed concentration of PADI4 (2.8 μM in protomer units). The samples were prepared the day before and left overnight at 5 °C; before the measurements, they were incubated for 1 h at 25 °C. Experiments were carried out in the same buffer used for the steady-state experiments. The samples were excited at 280 and 295 nm, and the rest of the experimental set-up was the same described above. In all cases, the appropriate blank-corrections were made by subtracting the signal obtained with the corresponding amounts of RYBP by using the software KaleidaGraph (Synergy software, Reading, PA, USA). Spectra were corrected for inner-filter effects during fluorescence excitation [65]. The titration was repeated three times, using new samples; variations in the results were lower than 10 %.

The dissociation constant of the corresponding complex, K_d, was calculated by fitting the binding isotherm constructed by plotting the observed fluorescence change as a function of RYBP concentration to the general binding model, explicitly considering protein depletion due to binding [66,67]:

$$F = F_0 + \frac{\Delta F_{max}}{2[PADI4]_T}\left([\mathrm{RYBP}]_T + [\mathrm{PADI4}]_T + K_d\right) - \sqrt{\left(\left([\mathrm{RYBP}]_T + [\mathrm{PADI4}]_T + K_d\right)^2 - 4[\mathrm{RYBP}]_T[\mathrm{PADI4}]_T\right)} \quad (1)$$

where F is the measured fluorescence at any particular concentration of RYBP after subtraction of the spectrum of the sample containing only the same concentration of such protein (*i.e.*, F is the differential, or difference fluorescence); ΔF_{max} is the largest change in the fluorescence of RYBP when all polypeptide molecules were forming the complex, compared to the fluorescence of each isolated protein (at the same corresponding concentration); F_0 is the fluorescence intensity when no RYBP was added; $[\mathrm{PADI4}]_T$ is the constant, total concentration of PADI4; and $[\mathrm{RYBP}]_T$ is that of RYBP, which was varied during the titration. Fitting to Eq. (1) was carried out by using KaleidaGraph (Synergy software, Reading, PA, USA).

2.8. Circular dichroism (CD)

The steady-state far-UV CD spectra were collected on a Jasco J810 spectropolarimeter (Jasco, Tokyo, Japan) with a thermostated cell holder and interfaced with a Peltier unit. The instrument was periodically calibrated with (+)-10-camphorsulfonic acid. A cell of path length 0.1-cm was used (Hellma, Kruibeke, Belgium). Spectra were corrected by subtracting the corresponding baseline. Protein concentrations and buffers were the same used in the fluorescence experiments, as well as the protocol for sample handling before acquiring the spectra. Spectra of each isolated macromolecule and that of the complex were acquired at 25 °C as an average of 6 scans, at a scan speed of 50 nm/min, with a response time of 2 s and a band-width of 1 nm.

2.9. Isothermal titration calorimetry (ITC)

Calorimetric titrations for assessing the interaction of PADI4 with RYBP were carried out in an automated high-sensitivity Auto-iTC200 calorimeter (MicroCal, Malvern-Panalytical, Malvern, UK). Experiments were performed at 25 °C in 20 mM Tris buffer (pH 7.5), 5 mM TCEP, 150 mM NaCl and 5 % glycerol at 25 °C. PADI4 (100 μM in protomer units) in the injection syringe was titrated into the RYBP solution (10 μM) in the calorimetric cell. A series of 19 injections with 2 μL volume, 0.5 μL/s injection speed, and 150 s time spacing was programmed while maintaining a reference power of 10 μcal/s and a stirring speed of 750 rpm. The heat effect *per* injection was calculated by integration of the thermal power raw data after baseline correction, and the interaction isotherm (ligand-normalized heat effect *per* injection as a function of the molar ratio) was analyzed by non-linear least-squares regression data analysis, applying a model that considers a single binding site to estimate the association constant, K_a; the interaction enthalpy, ΔH; and the stoichiometry of binding, n (although, in practice, the apparent stoichiometry n usually reports the fraction of active protein in the calorimetric cell). The dilution injection heat (reflecting any unspecific phenomenon such as solute dilution, buffer neutralization, temperature equilibration or solution mechanical mixing) was accounted for by including an adjustable constant parameter in the fitting. Due to the presence of glycerol in solution and a potential minor mismatch in glycerol concentration between cell and syringe solutions, the background injection heat was large. Data analysis was conducted in Origin 7.0 (OriginLab, Northampton, MA, USA) with user-defined fitting functions.

2.10. Structure prediction and modeling

In order to gauge the structural nature of the interaction between RYBP and PADI4 molecules, we used the deep-learning-based program AF2 [68,69] to predict the likely mode and stoichiometry of assembly. The holo-protein model structure of human RYBP deposited in the AF2 model database (UniProt identifier Q8N488, with a corresponding model structure at https://alphafold.ebi.ac.uk/entry/Q8N488) [70] reveals a largely disordered, 228-residue-long chain with two small, embedded protein modules with high confidence metric (pLDDT, predicted local distance different-test) folds: an N-terminal Zn-finger domain followed by a short α-helix (residues 23-71); and a C-terminal β-hairpin fold (residues 145-179) that has previously been captured bound to a C-terminal RING 1B domain (PDB identifier 3IXS, [71]). There is a human PADI4 model structure (UniProt Q9UM07, AF2 database https://alphafold.ebi.ac.uk/entry/Q9UM07) showing a distinctive 3-lobed architecture – the catalytic domain preceded by two immunoglobulin-like modules in a linear arrangement – and it has been extensively studied by X-ray crystallography as a homodimer in complex with substrate analogs and small molecule compounds [72–74].

For studying the binding of RYBP to PADI4, we used AF2-multimer [68,69] (version 2.3.1, implemented within ColabFold1.5.2; https://github.com/sokrypton/ColabFold [75]). This algorithm was applied to

pair human RYBP with PADI4, iteratively narrowing the interaction to an N-terminal region of RYBP (containing the Zn finger module) and the catalytic C-terminal domain of PADI4. The resulting ensemble of top-ranked models (by interface pTM or ipTM metric, relaxed by Amber within ColabFold to clean up potential side-chain clashes) showed consistent docking of the Arg53-bearing loop into the PADI4 active site. The resulting structures were manipulated and visualized within PyMOL 2.5.4 (https://www.pymol.org).

The results of AF2 were also confirmed by using the protein-protein docking algorithm ClusPro [76] by performing a blind docking with either the basic 'electrostatic-favored' scoring schemes (which is the most appropriate for modeling the binding of IDPs, such as RYBP), or the mixed 'van der Waals + electrostatics' scheme (which does not apply the pairwise potential that accounts for desolvation contributions in the protein association). The docking poses were also rescored by using a more accurate molecular mechanics (MM) method, with the generalized Born surface area (MM/GBSA) continuum solvation [77] as implemented in the web server HawkDock [78]. Interactions were calculated after 5000 steps of energy minimization, by using the Amber ff02 force field and the implicit solvent GB^{OBC1} model with interior dielectric constant $\varepsilon_{in} = 1$ [79].

2.11. Statistical analysis

Results in the combined therapy consisting in the simultaneous administration of two drugs are shown as the mean ± standard deviation (SD) of three independent experiments. To evaluate the normal distribution of the data, the Shapiro–Wilk statistical test was used; either the Student's *t*-test or the Mann–Whitney *U* test were used to analyze the association between variables. Differences were considered to be statistically significant with a *p*-value <0.05. Statistical analysis was performed with GraphPad Prism v7.0a software (GraphPad Software Inc., San Diego CA, USA).

3. Results

3.1. Binding of PADI4 to RYBP occurred in cellulo in the cytosol and nucleus

It has been described that RYBP is a multifunctional protein with a ubiquitin-binding function that preferentially binds to K63-linked ubiquitin chains [80], RING 1B, histone H2A, and other transcription factors [81,82,83] with great relevance in cancer. On the other side, PADI4 has been reported to have relevance in cancer by binding to PKP1, Impα3, NUPR1 [52–54], but also to histone H3 [84]. Given the importance of both proteins, RYBP and PADI4, in cancer development and their interactions with the histones, we first wondered about their common cellular localization in different cancer cell types. The IF experiments in HGUE-GB-42 GBM cell line; in SW-480, isolated from the large intestine of a Dukes C colorectal cancer patient; and in RWP-1, as a model of pancreatic cancer, showed that both proteins were expressed and colocalized in the same cellular compartments (Fig. S1). As expected, both proteins had a prominent nuclear staining, as shown by the colocalization with DAPI, but we could also detect some staining in the cytoplasm (Figs. S1 and S2). These data suggest that they may interact within the nuclear compartment of the different cell lines.

To test whether or not PADI4-RYBP interaction occurred endogenously within those cancer cells, we used the Duolink *in situ* assay. This

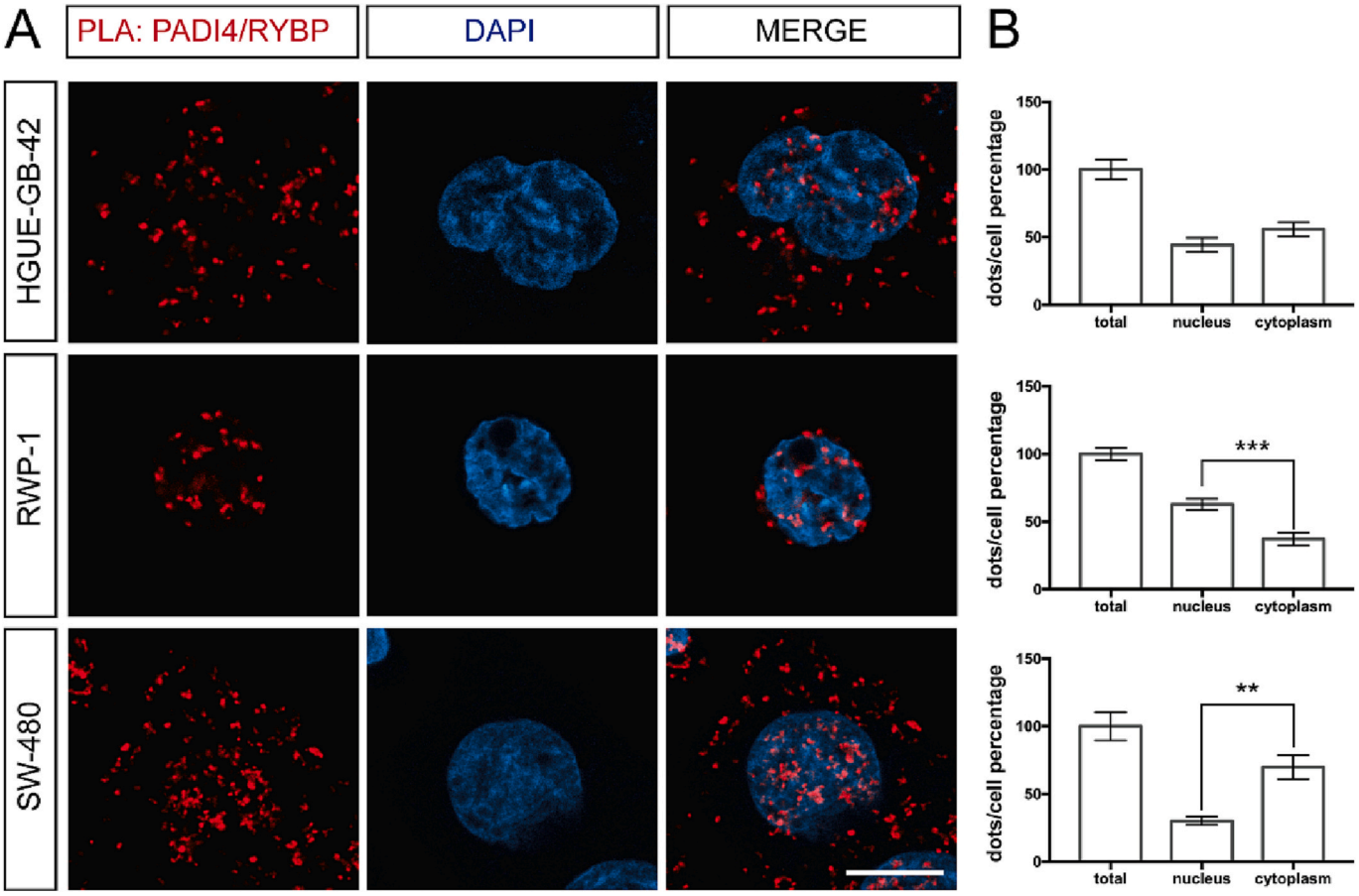

Fig. 1. RYBP interacted with PADI4 *in cellulo*. (A) PLAs of PADI4 with RYBP reveal the interaction between the two proteins in different patient-derived cells. A representative experiment is shown (n = 5). Scale bar = 20 μm. (B) Counting of the red dots. The Fiji software was used to count the number of red dots. Data represent mean ± SEM, Student's 2-tailed unpaired *t*-test was used, $^{**}p < 0.01$; $^{***}p < 0.001$.

technique, known as PLA, resolves the binding of proteins that occurs at distances shorter than 16 Å. In contrast to what we could expect after the results of the IF experiments, the majority of the red fluorescent spots, corresponding to the PLA signals, indicated that PADI4 interacted with RYBP not only within the nucleus but also in the cytosol, regardless of the cancer cell type (Figs. 1 and S3). PLA is a technique that resolves binding, and it is more sensitive than immunocytochemistry. Then, it is not surprising that it can more efficiently detect the binding of two proteins (and thus, complex formation) in any cellular compartment.

To sum up, our results indicate that PADI4 and RYBP interacted in the different compartments of cancer cells obtained from several tissues.

3.2. Reduction of PADI4 binding to RYBP upon PADI4 inhibition is cancer-type dependent

GSK484 is an enzymatic inhibitor of PADI proteins that has shown a strong preference for PADI4 over the other isozymes [85]. We wondered whether the presence of this inhibitor decreased the formation of the PADI4/RYBP complex.

After 24 h treatment with 20 μM of GSK484, PLAs showed the decrease in the number of red dots, and further indicating that the interaction between PADI4 and RYBP, occurred mainly in the nucleus as shown by DAPI nuclear counterstaining (Figs. 2A and S4). Interestingly, the reductions in the populations of formed PADI4/RYBP complexes were not the same in all cancer cell lines studied. While RWP-1 showed the greatest decrease in the number of dots *per* cell, HGUE-GB-42 and SW-480 presented a modest, but significant, reduction in PADI4/RYBP interaction (Figs. 2B and S4).

In conclusion, the binding between RYBP and PADI4 was affected by the administration of GSK484 (Figs. 2 and S4). As GSK484 is an enzymatic inhibitor of PADI4, our findings suggested that either RYBP could competitively bind to the active site of PADI4 and be citrullinated by the enzyme; or alternatively, the presence of the inhibitor could alter conformationally (*i.e.*, allosteric conformational change) the RYBP-binding site of PADI4.

3.3. Inhibition of PADI4 enhanced PARP inhibitor effects on pancreatic cancer cells

RWP-1 cells presented the strongest decrease in the population of PADI4/RYBP complexes formed at the nucleus, upon GSK484 treatment (Fig. 2). There are many PARP inhibitors, but DPQ has shown to enhance

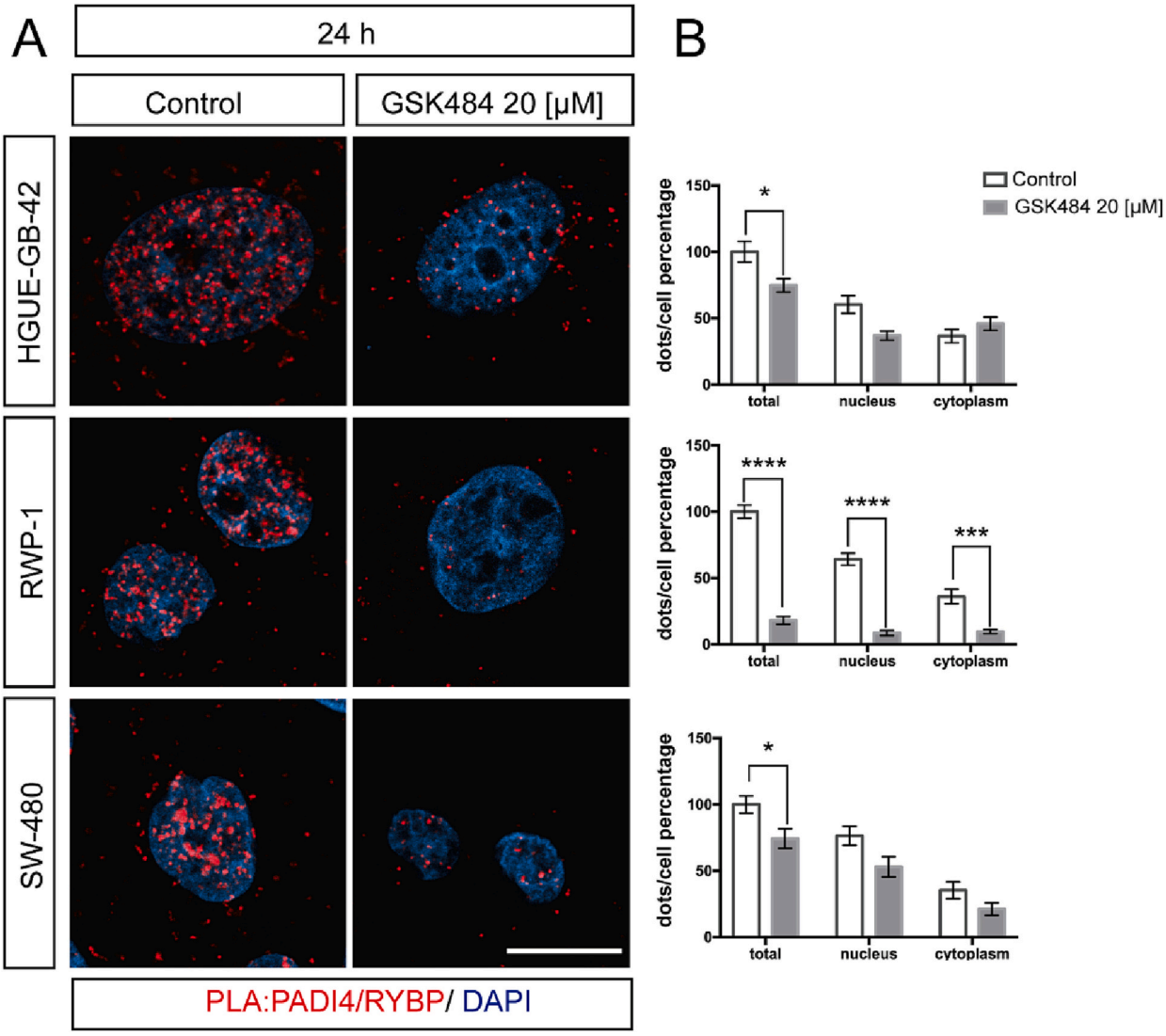

Fig. 2. The formation of the PADI4/RYBP complex was inhibited by the presence of GSK484. (A) PLA was performed in HGUE-GB-42, RWP-1 and SW-480 cells in the absence or the presence of GSK484 at a concentration of 20 μM, for 24 h. A representative experiment is shown ($n = 5$). Scale bar = 20 μm. (B) The Fiji software was used to count the number of red dots. Data represent mean ± SEM, 1-way ANOVA, Tukey's *post hoc* test was used, $^{*}p < 0.05$, $^{***}p < 0.001$; $^{****}p < 0.0001$.

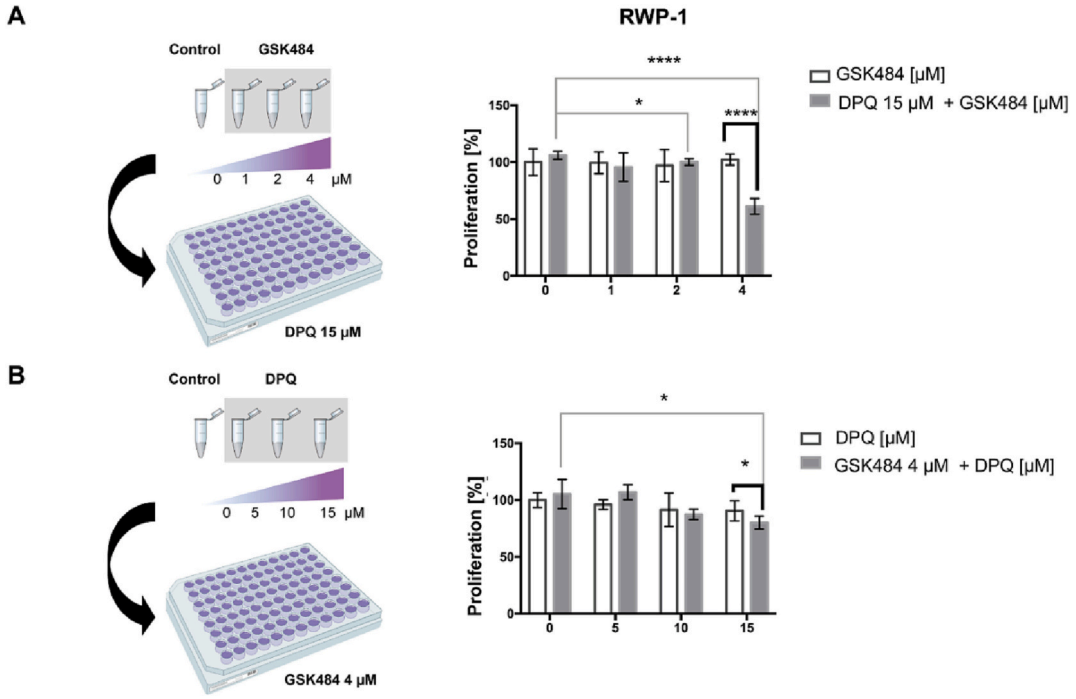

Fig. 3. Combined effect of GSK484 and DPQ. (A) Scheme of the followed protocol and bar diagrams showing results of the cell proliferation assays by keeping a constant concentration of 15 μM of DPQ and increasing that of GSK484. (B) Scheme of the followed protocol, and bar diagrams showing results of the cell proliferation assays by keeping a constant concentration of 4 μM of GSK484 and increasing that of DPQ. The data shown in the combined (cocktail) therapy were normalized to the control of each treatment. Asterisks indicate the statistical significance of the results ($*p < 0.05$, $****p < 0.001$).

the effect of the enzymatic therapy based on CLytA-DAAO in RWP-1 cells [86]. Therefore, we speculated that the treatment of these tumor cells with GSK484 could also be enhanced by the presence of DPQ. To see how single treatments affected RWP-1 cell line proliferation, we performed monotherapy experiments with each of the two drugs (Fig. 3A, B). First, we observed that a range of GSK484 concentration between 1 and 4 μM resulted in a decrease of the proliferation of RWP-1 cells (Fig. 3A). We observed that DPQ concentrations ranging between 1 and 15 μM did not significantly reduce its proliferation (Fig. 3B).

To test whether increasing concentrations of GSK484 could be affected by the presence of a constant amount of DPQ, we treated the cells in the presence of 15 μM DPQ with increasing GSK484 concentrations between 1 and 4 μM (Fig. 3C). Our experiments showed that the cocktail treatment of RWP-1 cells resulted in a significant decrease in cell proliferation, which was higher than in the GSK484 monotherapy (Fig. 3A, C). Similarly, to test whether DPQ could enhance the effect of GSK484 on RWP-1 proliferation, we treated the cells at a GSK484 4 μM constant concentration, with increasing concentrations of DPQ ranging from 1 to 15 μM. These experiments resulted in a statistically significant decrease in cell proliferation, demonstrating the synergistic effect of both drugs (Fig. 3A and B). Moreover, according to these results, the addition of DPQ seems to sensitize the cancer cells for the action of GSK484, suggesting that the most efficient way to apply this therapy would be to first administer the PARP inhibitor, and next the PADI4 inhibitor. These findings open the venue for new treatments in pancreatic cancer based on the additive effect that PADI4 enzymatic inhibition might have, in combination with other approved drugs.

3.4. PADI4 was bound to RYBP in vitro

As the *in cellulo* experiments indicated unambiguously that there was binding between RYBP and PADI4, we tested whether PADI4 interacted with RYBP *in vitro*, by following a two-part experimental approach. First, we used steady-state fluorescence and far-UV CD as spectroscopic techniques to monitor the binding and the possible concomitant conformational changes in the macromolecules; and second, we used fluorescence and ITC to quantitatively measure the thermodynamic parameters of such binding.

We used fluorescence to find out whether there was a change in: (i) the position of the maximum wavelength; (ii) the intensity at that wavelength; or (iii) both parameters, when the spectrum of the complex was compared to that obtained from the addition of the spectra of the two isolated proteins. A variation in fluorescence intensity by excitation at 280 nm was observed when the complex of PADI4 with RYBP was formed (Fig. 4A), but there were no changes in the maximum wavelength of the spectrum (which remained at ~340 nm).

Next, we carried out far-UV CD measurements, trying to confirm the fluorescence binding results. The CD spectrum of isolated RYBP at this pH had a minimum negative ellipticity at ~200 nm, characteristic of either random-coil polypeptide chains or denatured proteins (Fig. S5A) [87]. The spectrum had a shoulder at ~222 nm, which suggests the presence of α-helix- or turn-like conformations, but the contribution of aromatic signals of the protein at this wavelength could not be ruled out [87]. The estimated population of α-helix- or turn-like conformations was 5.5 %, as obtained from value of the molar ellipticity at 222 nm [15]; a similar result (9.5 %) was obtained when using the k2D software [88] to deconvolute RYBP spectrum. The spectrum of isolated PADI4 (Fig. S5B) corresponds to that of an α/β protein [51].

In agreement with the findings obtained by fluorescence, the addition far-UV CD spectrum, obtained from the sum of the spectra of isolated RYBP and PADI4, was different from that of the complex of the two proteins (Fig. 4B). Then, we can conclude that there were changes in the secondary structure of PADI4 and/or in that of RYBP when the two proteins were bound; however, we cannot rule out that the changes observed were due to displacements of some aromatic residues (or interactions involving these residues) of at least one of the two proteins. Since RYBP in isolation was disordered (Fig. S5A), we hypothesized that this chain could be ordered upon binding to PADI4. However, because of the nature of the variations observed in the far-UV CD spectrum, we cannot say which type of ordering is taking place, or even if the changes

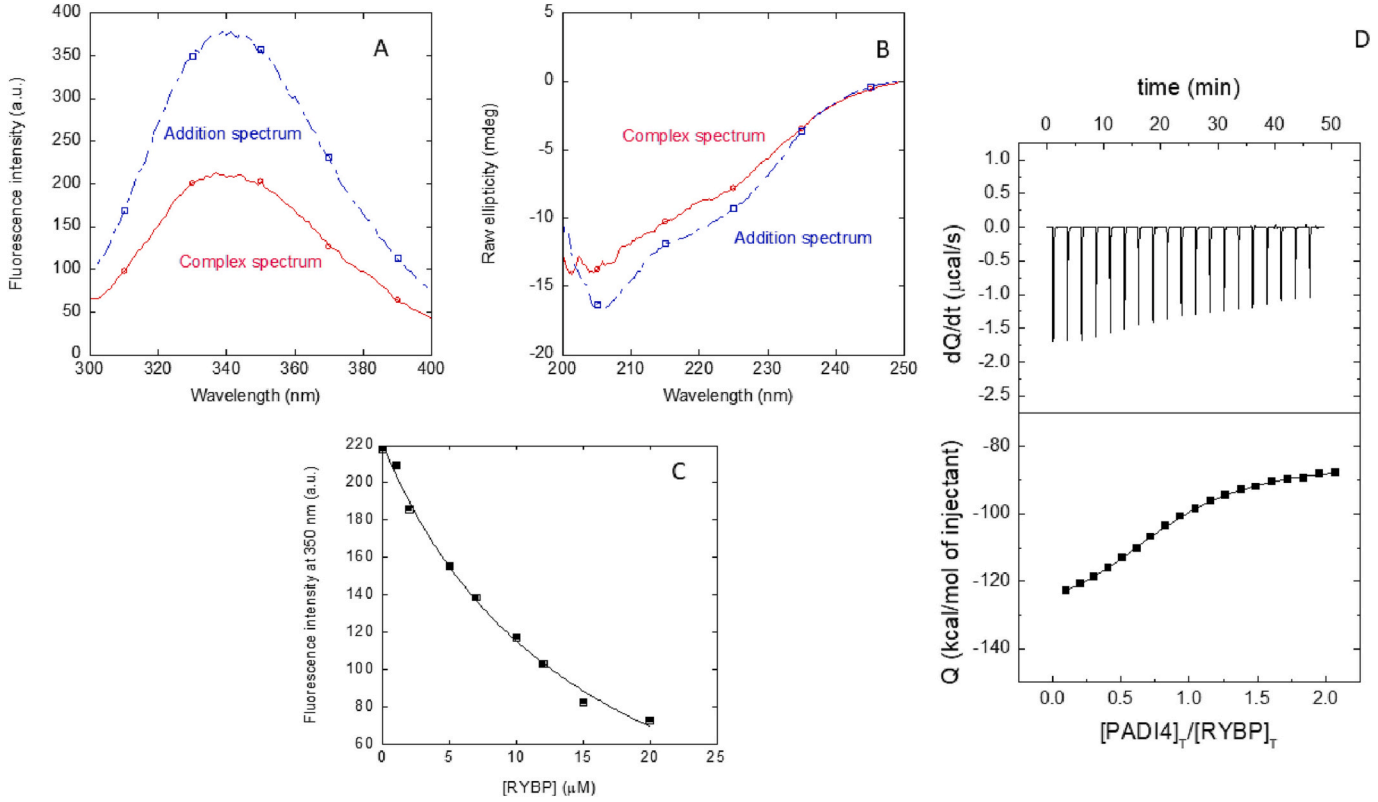

Fig. 4. Binding of RYBP to PADI4 as monitored by several biophysical probes. (A) Fluorescence spectrum obtained by excitation at 280 nm of the PADI4/RYBP complex, and addition spectrum obtained by the sum of the spectra of the two isolated macromolecules. (B) Far-UV CD spectrum of the PADI4/RYBP complex, and addition spectrum obtained by the sum of the spectra of the two isolated macromolecules. (C) Titration curve monitoring the changes in the fluorescence at 350 nm when RYBP was added to a solution containing PADI4. The fluorescence intensity on the y-axis is the relative signal after removal of the corresponding blank. The line through the data is the fitting to Eq. (1). Experiments were carried out at 25 °C. (D) Calorimetric titrations for the PADI4 binding to RYBP. The upper panel shows the thermograms (thermal power as a function of time), and the lower panel shows the binding isotherm (ligand-normalized heat effects per injection as a function of the molar ratio in the calorimetric cell). The continuous line corresponds to the fitting curve according to a single ligand binding site interaction model. Experiments were carried out at 25 °C.

observed are simply a rearrangement of some of the aromatic side-chains. It could be thought that the differences of the spectrum of the complex and that of the isolated PADI4 could provide evidence on the ordering of RYBP upon binding, but the fact that the positions of some aromatic residues change, when the two proteins are bound (as suggested by the fluorescence and *in silico* results (Section 3.5)), precludes to draw any further conclusion.

As we observed changes in the fluorescence spectra upon PADI4 binding to RYBP, to determine the affinity constant, we carried out titrations by keeping constant the concentration of PADI4, and increasing that of RYBP. The results provided a K_d value of 15 ± 10 μM (Fig. 4C) for the interaction between both proteins. We also used ITC to determine the binding parameters (Fig. 4D). The results indicated that the interaction was highly exothermic (favorable enthalpic contribution and unfavorable entropic contribution to the Gibbs energy of binding), with $\Delta H = -42$ kcal/mol, and the K_d was 1.1 ± 0.2 μM, lower than the value obtained by fluorescence. The stoichiometry of the reaction was 0.85, indicating that the dimer of PADI4 was bound to two molecules of RYBP. It could be thought that the values obtained by the two different techniques are quite different, but it must be kept in mind that fluorescence spectroscopy is a steady-state technique (reactant molecules are incubated for a period of time and the equilibrium state is assayed), and ITC is a transient-effect technique (reactant molecules are mixed and the transient effect is observed for a couple of minutes after each injection). This can lead to different estimates of the K_d. Moreover, the uncertainty in these estimates is quite different: 67 % is the relative error for the dissociation constant estimated by spectroscopy, and 18 % is the relative error for the dissociation constant estimated by calorimetry. Taking all this into consideration, although the values may appear quite different, they both are in the low micromolar range. Besides, the purpose of these measurements was to provide direct evidence of the interaction between RYBP and PADI4, providing an approximate estimate (in a broad sense) of the K_d for such interaction, and to compare such strength with that of other interactions where PADI4 is involved.

To sum up, we conclude that RYBP was bound to PADI4, with a dissociation constant in the low micromolar range, and involving the tryptophans of at least one of the two proteins.

3.5. Modeling of the PADI4/RYBP complex

The binding of RYBP to PADI4 was investigated by using molecular docking, starting with the algorithm AF2-multimer [68,69]. This multimer application of AF2 has proven to be one of the most accurate tools to model protein complexes, including ligand-receptor binding interfaces [68]. In an unbiased fashion, the full-length protein chains of human RYBP and PADI4 (at a 1:1 and 2:2 stoichiometry) were queried for binding by AF2.3.1 as implemented on ColabFold 1.5.2 in template-free mode [75]. It was immediately clear that the interaction centered on a structured loop in RYBP between Zn-finger and its predicted proximal helix (residues 50-54), and the catalytic pocket of PADI4. This suggests that RYBP binding mimics the docking of peptide substrates to PADI4 [72,74]. To better assess the interface (and ease the computational burden), we henceforth focused on an RYBP fragment that contains the N-terminal folded module (residues 17-72), trained against the catalytic domain of PADI4 (residues 294-663). The resulting top-ranked models converge on the RYBP loop formed by residues STRKP (residues

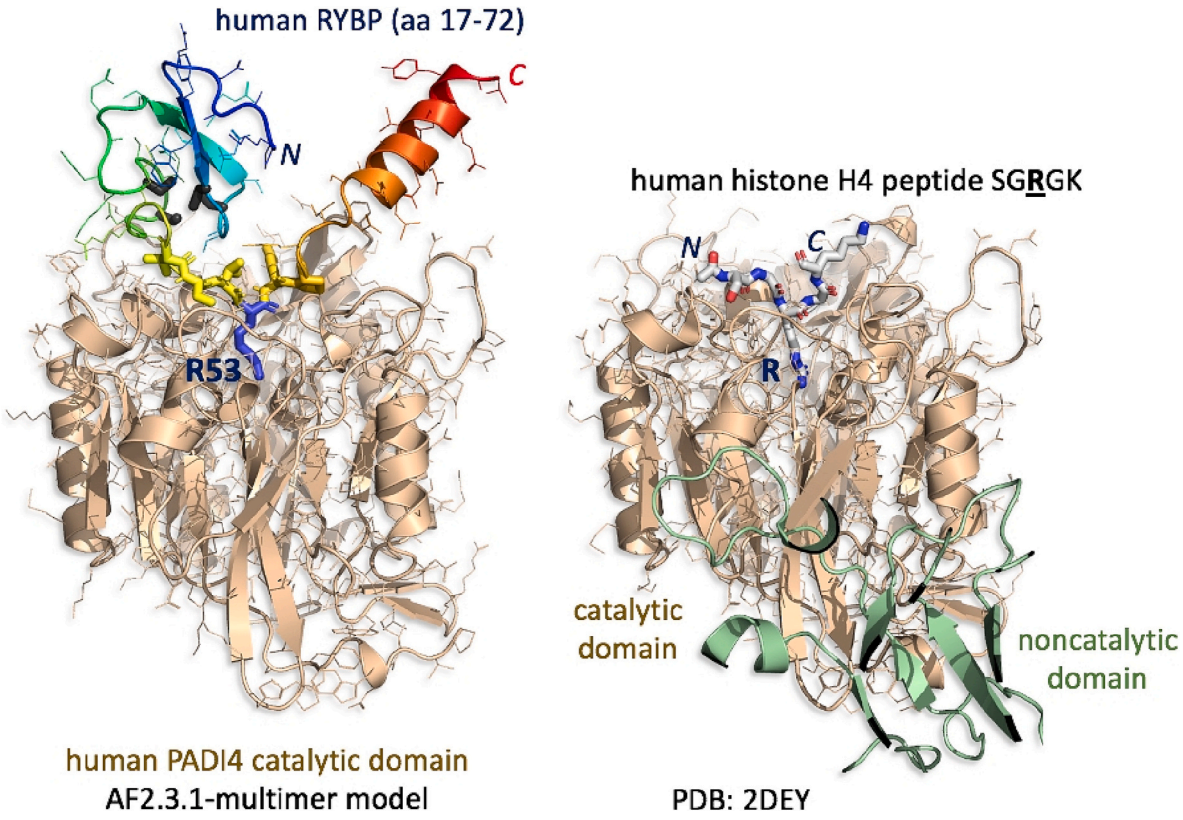

Fig. 5. Modeling of the PADI4/RYBP complex. Comparative structures of the AF2.3.1-multimer-generated model of the RYBP residue 17-72 fragment (colour-ramped from blue N-terminus to red C-terminus) encasing the Zn-finger module at top left (with metal-coordinating Cys side-chains in black stick form) and a following short helix at top right (in orange and red). The docked loop in yellow (amino acids TSTRKP, side-chains in stick form) buries the central Arg53 in the wheat-colored PADI4 catalytic pocket. To the right is the X-ray structure of human PADI4 bound to a histone H4 peptide SGRGK (representing the visible portion of a larger 10-mer peptide), with buried central arginine labeled (PDB identifier: 2DEY, [89]).

51-55, with buried Arg53 side-chain) docked to PADI4. This model can be closely superimposed with that of the histone H4 N-terminal substrate peptide SGRGK docked to the PADI4 catalytic pocket from the 2DEY PDB structure at 2.25 Å resolution [89] (Fig. 5).

The protein-protein docking algorithm ClusPro [76], together with the generalized Born surface area (MM/GBSA) continuum solvation method implemented in the web server HawkDock [78], were used to further support these findings, and to obtain a more accurate estimate of the binding affinity of the two proteins. In fact, AF2-multimer explicitly encourages a combined use with ClusPro, both to validate the results and to refine them [70]. In our specific case, the use of this algorithm was convenient also because it allowed us to select an 'electrostatic-favored' scoring scheme that is particularly appropriate for IDPs (such as RYBP), due to their sensitivity to Coulombic interactions in driving the association to molecular partners. The results of the blind docking of the RYBP fragment 17-72 (Table 1) confirmed that the best poses (Table 1) involved the arginine residues of RYBP closely grouped around residue Arg53 (*i.e.*, Arg47, Arg53 and Arg56). They interacted with a number of prevalently acidic residues of PADI4, centered around the key residue Cys645 in the catalytic site of the citrullinating enzyme (Fig. 6).

It is interesting to note that slightly less favorable but qualitatively similar predictions were obtained by ClusPro also with a mixed 'van der Waals + electrostatics' scheme (see again Table 1). This option still accounts for Coulombic interactions, but zeroes the desolvation contributions to the binding energy, suggesting that shape complementarity of the binding hot spot regions of the two proteins plays a minor role in their association [76]. This observation indicates that the binding of the loop region 51-55 of RYBP is not penalized with respect to other more structured protein regions, further supporting the prediction of the anchoring of such a flexible region to PADI4.

The fact that at least one arginine residue of RYBP is directly involved in the binding to the catalytic site of PADI4 supports *in cellulo* competitive binding results regarding GSK484 (Fig. 2), suggesting that RYBP might be a substrate for PADI4. The docking model suggested that neither Trp25 nor Tyr70 of RYBP changed very much their positions in the complex, when compared to those in the unbound species. However, Phe314 of PADI4 changes its conformation and packing with respect to Tyr636 of PADI4, pointing to the side-chain of Arg47 of RYBP. These changes of the aromatic side-chains could explain some of the variations observed in the far-UV CD spectra (Fig. 4B).

4. Discussion

Decreases in RYBP levels in cells have been related with the development of several types of cancers [2, and references therein]. Furthermore, the genomic region containing the *RYBP* gene (3p13-14) is deleted in different tumor types [90,91]. The deletion of this chromosomal region is associated with a worse prognosis compared to patients without such obliteration. Besides, the decreased levels of RYBP in patient tumor samples, cell lines and mouse xenografts seem to be correlated with increased disease severity and shorter survival times in GBM, lung, breast cervical and hepatocellular cancers [2]. As RYBP is an ubiquitin-binding protein, it is involved in the regulation of p53 by its stabilization. Thus, a great knowledge of the proteome of RYBP will allow to elucidate in full all the protein cascades where it intervenes and whether its involvement in such pathways could provide new targets for drug design. In this work, we hypothesized that RYBP could interact with PADI4 since it is also involved in p53-gene expression, as well as in the expression of other p53-target genes [48–50]. In addition, both proteins intervene in pathways where glycogen synthase kinase 3β

Table 1
Binding affinity of the fragment containing the N-terminal folded module of RYBP (residues 17-72) and the catalytic domain of PADI4 (residues 294-663), estimated by using the MM/PBSA technique on the docking poses obtained with the algorithm ClusPro.

Scoring scheme	Pose rank	Binding affinity (kcal/mol)	Residues most contributing to binding affinity (kcal/mol)	
			PADI4	RYBP
Electrostatic-favored	1	–90.52	Met343 (–5.81), Glu317 (–5.46), Glu315 (–4.15)	Arg56 (–14.25), Arg53 (–7.84), Pro55 (–4.77)
	2	–74.44	Asp344 (–5.90), Asp345 (–5.76), Ile638 (–5.29)	Arg53 (–8.04), Glu37 (–6.08), Phe39 (–4.52)
	3	–85.05	Asp344 (–10.11), Phe576 (–6.41), Glu339 (–5.27)	Arg53 (–12.16), Arg56 (–7.49), Arg47 (–7.19)
van der Waals + electrostatics	1	–72.45	Phe314 (–5.82), Glu339 (–4.53), Glu341 (–3.43)	Arg53 (–13.14), Thr52 (–8.73), Lys48 (–6.14)
	2	–81.22	Glu340 (–8.34), Glu339 (–6.64), Glu317 (–4.59)	Arg56 (–12.17), Arg47 (–8.57), Arg53 (–5.84)
	3	–69.12	Asp344 (–8.08), Glu339 (–6.46), Gln346 (–4.58)	Arg56 (–8.49), Arg53 (–7.61), Arg47 (–6.97)

(GSK-3β) mediates: the citrullination of such protein by PADI4 triggers epithelial-to-mesenchymal transition in breast cancer cells [92] and RYBP interact with several routes involving the kinase ATM and GSK-3β [24].

To test the hypothesis of a well-defined and well-formed complex between PADI4 and RYBP, we carried out biological experiments in several cancer lines (as both proteins intervene in the development of several cancer types), as well as *in vitro* experiments. IF and PLA experiments showed the co-localization and the binding of both proteins. The decrease in the population of the complex formed between the two proteins, triggered by the presence of GSK484, suggested that RYBP was bound to the active site of the enzyme; or alternatively, the presence of the PADI4-inhibitor caused allosteric changes in the RYBP-binding region of PADI4. However, the blind *in silico* experiments seem to rule out the allosteric conformational changes, pinpointing RYBP as a likely substrate of PADI4.

However, it is important to stress out that the fact that the *in silico* results suggest that binding occurs at the active site of PADI4, it is not an unambiguous proof of the citrullination of RYBP. We have not been able to detect citrullinated RYBP *in cellulo*, and then, all we can conclusively state from our studies is the presence of binding between the two proteins in several cancer cells. It is true, from our experiments, that the use of PADI4 inhibitor, GSK484, hampers binding (with variations among the cells, although it could be due to the different metabolism among the several cancer types) between PADI4 and RYBP. The binding of RYBP to

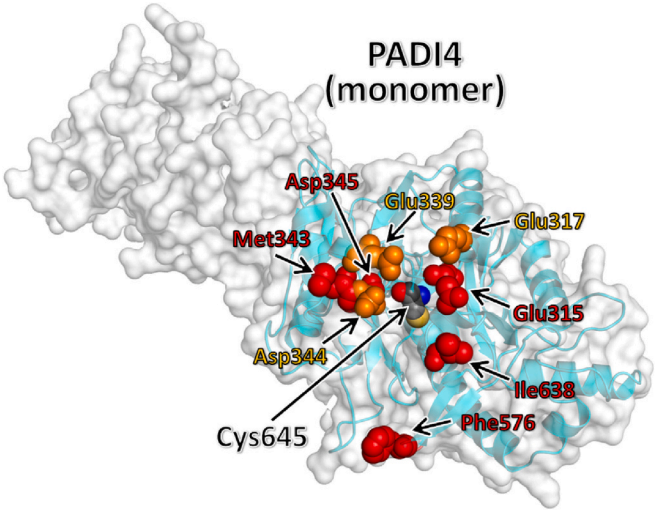

Fig. 6. PADI4 binding interface with RYBP as predicted by molecular docking. The binding to the catalytic domain of PADI4 (ribbon representation, cyan) of the RYBP fragment 17-72 was simulated. Residues of PADI4 that contribute the most to the association of RYBP (Table 1) are estimated by using the MM/PBSA technique on the docking poses obtained with the algorithm ClusPro. The residues found (sphere representation) are mapped on a single monomer of PADI4, and center around the key residues Cys645 in the catalytic site. They were obtained either solely with an 'electrostatic-favored' scoring scheme (red), or both with it and a mixed 'van der Waals + electrostatics' scoring scheme (orange).

a region different to the one we predicted could still be possible in the case the docking of the GSK484 in the active site of PADI4 hampers it by an allosteric rather than a direct competitive effect. Therefore, we can only conclude from our studies that there is binding between the two proteins *in vitro* and *in cellulo*, but we cannot conclude unambiguously, based only on the *in silico* results, that RYBP is a substrate of PADI4.

It has been shown that RYBP sensitizes cancer cells to PARP inhibitors [93]. There are PARP inhibitor drugs that have been approved as a cancer treatment, and others that are used in combination with chemo and/or radiotherapy to enhance the therapeutic effects [94]. PARP-1 participates in the DNA base excision repair system. However, PARP has a dual function: when DNA is strongly damaged, it activates a cell death mechanism; but if the damage is mild, PARP binds to the region where the damage has occurred and it recruits enzymes responsible for DNA repair [94]. Therefore, PARP inhibitors can increase survival in patients with cancers that are highly dependent on PARP activity, but they can also enhance the action of other treatments that act by damaging DNA. PARP-1 inhibitors have been shown to be useful in the treatment of breast cancer with BRCA1 and BRCA2 mutations [95,96]. The products of these two genes are involved in the homologous recombination that occurs during the repair of double-stranded DNA, and, therefore, the phenomenon known as synthetic lethality occurs when inhibiting other DNA repair systems with PARP1 inhibitors [97]. In the mitochondrion, the sugar PAR-polymer binds to the apoptosis inducing factor protein and causes its nuclear translocation, initiating large-scale DNA fragmentation and chromosome condensation [94]. In this work, we observed that the combined effect of DPQ, a PARP inhibitor, and GSK484, a PADI4 inhibitor, on cell proliferation was higher than the respective monotherapies for both drugs in RWP-1 cancer cells.

We speculated that the PADI4-binding region of RYBP seems to be the N-terminal region, where the Zn-finger is located and theoretical predictions indicate a local folded structure in the otherwise disordered chain; furthermore, our findings seemed to be the first evidence of this region being involved in recognition of other proteins. We hypothesize, on the basis of our *in silico* results, that RYBP might be a non-histone

substrate for PADI4, which could add to the well-known list of substrates of the PADI4 enzyme, such as ING4, p300 or GSK3β [73]. The use of a PADI4 inhibitor in the modification of cellular processes is not new; for instance, in several PADI4-overexpressing cancer cells, the use of PADI4 enzymatic inhibitors or PADI4 siRNA resulted in apoptosis and cell cycle arrest [98].

The dissociation constant (1 μM, as measured by ITC) is within the same range of those found for other partners of PADI4: NUPR1 (18 ± 6 μM) [54], for PKP1 (14 ± 0.2 μM) [53] and Impα3 (4.8 ± 0.9 μM) [52]. These results suggest that no matter how ordered the protein partner or substrate of PADI4 is (for instance, NUPR1, as well as RYBP, is an IDP), the affinity for that companion is similar in all cases so far. This means that the affinity of all of them for PADI4 is not very large probably to allow for its involvement in transient interactions along several protein routes.

Given the different PTMs that can affect and regulate RYBP [2], it would not be surprising that RYBP might also be citrullinated, but at the moment, we cannot prove unambiguously this hypothesis. Our initial goal was to probe the presence of an interaction between PADI4 and RYBP, and because of the *in cellulo* results with the GSK484 and the *in silico* findings, we suggested that citrullination of RYBP could be involved. The possibility of the enzymatic conversion of an arginine residue into a citrulline in RYBP would result in the loss of a positive charge of molecules. Then, citrullination would perturb several intra- and intermolecular electrostatic interactions, causing partial unfolding leading to conformational changes in RYBP [37]. As a consequence, RYBP may become more immunogenic, inducing an autoimmune response as it happens with many other citrullinated proteins [37,99]. Citrullination could alter the binding of RYBP to K63-linked ubiquitin chains, RING1B, histone H2A and other transcription factors [100]; if the ability to bind K63-ubiquitin chains is hampered by citrullination, the removal of RYBP from DNA damage active sites at sites of DSBs would not be possible [22]. Furthermore, impediment of the RYBP-ubiquitin-binding abilities would result in the impossibility of the breast cancer gene 1 complex recruitment [2]. RYBP also compacts efficiently chromatin [101], and citrullination could impede such process. RYBP has also been shown to intervene in apoptosis through the interaction with MDM2, SKP1, Cullin-1, HIPPI or Ring1B proteins [2,34]. Then, possible citrullination at the RYBP-binding sites of those protein could result in the absence of such key event in the development of cancer.

Taken together, our study opens up venues for understanding the basis of possible molecular mechanisms in different types of cancer and for the development of new applications based on PADI4 interaction with RYBP.

CRediT authorship contribution statement

Conceptualization, JLN, BR, CdJ, JFB, MS and AVC; methodology, SAA, MFB, JLN, CdJ, AVO, BR, JFB and AVC; investigation, SAA, MFB, MS, JFB, BR, AVO, AVC and OA; data formal analysis, SAA, MFB, AVO, JLN, BR, JFB, OA, and AVC; writing-original draft preparation, SAA, JLN, CdJ, MS, JFB and AVC; materials, JLN, CdJ, MV, EF, JFB, OA and AVC; writing-review and editing, SAA, MFB, MS, JLN, CdJ, BR, JFB, EF, MV, OA and AVC; funding acquisition, JLN, CdJ, OA, EF, MS, and AVC.

All authors have read and agreed to the published version of the manuscript.

Declaration of competing interest

The authors declare that they have no known competing financial interests or personal relationships that could have appeared to influence the work reported in this paper.

Data availability

Data and materials are available from the corresponding authors upon reasonable request.

Acknowledgements

This research was funded by Ministry of Science and Innovation MCIN/AEI/10.13039/501100011033/ and "ERDF A way of Making Europe" [PID2021-127296OB-I00 to AVC; and PDC2022-133952-I00 to EF]; by Instituto de Salud Carlos III co-funded by European Social Fund "Investing in your future" [CP19/00095 to CdJ] [PI22/00824 to MS and CdJ] [PI18/00394 to OA]; by Diputación General de Aragón ["Protein targets and Bioactive Compounds group" E45-20R to AVC, and "Digestive Pathology Group" B25-20R to OA], and by Consellería de Innovación, Universidades, Ciencia y Sociedad Digital (Generalitat Valenciana) [CAICO 2021/0135 to CdJ and JLN]. SAA was recipient of a "Carolina Foundation Predoctoral Fellowship 2020".

The funders had no role in the study design, data collection and analysis, decision to publish, or preparation of the manuscript.

We thank Patricia Santofimia-Castaño (INSERM, Marseille, France) for her help with the estimates of the Pearson correlation coefficients. We thank the two reviewers for helpful suggestions and discussion.

Appendix A. Supplementary data

There are five figures containing IF images of PADI4 and RYBP interaction (Fig. S1; S2);PLAs of both proteins under different conditions (Figs. S3 and S4); and the far-UV CD spectra of isolated RYBP and PADI4 under the same solution conditions (Fig. S5). Supplementary data to this article can be found online at https://doi.org/10.1016/j.ijbiomac.2023.125632.

References

[1] E. Garcia, C. Marcos-Gutiérrez, M. Del Mar Lorente, J.C. Moreno, M. Vidal, RYBP, a new repressor protein that interacts with components of the mammalian Polycomb complex, and with the transcription factor YY1, EMBO J. 18 (1999) 3404–3418, https://doi.org/10.1093/EMBOJ/18.12.3404.

[2] C.J. Simoes da Silva, R. Simón, A. Busturia, Epigenetic and non-epigenetic functions of the RYBP protein in development and disease, Mech. Ageing Dev. 174 (2018) 111–120, https://doi.org/10.1016/J.MAD.2018.03.011.

[3] I. Bajusz, S. Henry, E. Sutus, G. Kovács, M.K. Pirity, Evolving role of RING1 and YY1 binding protein in the regulation of germ-cell-specific transcription, Genes (Basel) 10 (2019), https://doi.org/10.3390/GENES10110941.

[4] Z. Gao, J. Zhang, R. Bonasio, F. Strino, A. Sawai, F. Parisi, Y. Kluger, D. Reinberg, PCGF homologs, CBX proteins, and RYBP define functionally distinct PRC1 family complexes, Mol. Cell 45 (2012) 344–356, https://doi.org/10.1016/J.MOLCEL.2012.01.002.

[5] M. de Napoles, J.E. Mermoud, R. Wakao, Y.A. Tang, M. Endoh, R. Appanah, T. B. Nesterova, J. Silva, A.P. Otte, M. Vidal, H. Koseki, N. Brockdorff, Polycomb group proteins Ring1A/B link ubiquitylation of histone H2A to heritable gene silencing and X inactivation, Dev. Cell 7 (2004) 663–676, https://doi.org/10.1016/J.DEVCEL.2004.10.005.

[6] W. Ma, X. Zhang, M. Li, X. Ma, B. Huang, H. Chen, D. Chen, Proapoptotic RYBP interacts with FANK1 and induces tumor cell apoptosis through the AP-1 signaling pathway, Cell. Signal. 28 (2016) 779–787, https://doi.org/10.1016/J.CELLSIG.2016.03.012.

[7] L. Zheng, O. Schickling, M.E. Peter, M.J. Lenardo, The death effector domain-associated factor plays distinct regulatory roles in the nucleus and cytoplasm, J. Biol. Chem. 276 (2001) 31945–31952, https://doi.org/10.1074/JBC.M102799200.

[8] A.A.A.M. Danen-van Oorschot, P. Voskamp, M.C.M.J. Seelen, M.H.A.M. van Miltenburg, M.W. Bolk, S.W. Tait, J.G.R. Boesen-de Cock, J.L. Rohn, J. Borst, M. H.M. Noteborn, Human death effector domain-associated factor interacts with the viral apoptosis agonist Apoptin and exerts tumor-preferential cell killing, Cell Death Differ. 11 (2004) 564–573, https://doi.org/10.1038/SJ.CDD.4401391.

[9] F.G. Gervais, R. Singaraja, S. Xanthoudakis, C.A. Gutekunst, B.R. Leavitt, M. Metzler, A.S. Hackam, J. Tam, J.P. Vaillancourt, V. Houtzager, D.M. Rasper, S. Roy, M.R. Hayden, D.W. Nicholson, Recruitment and activation of caspase-8 by the Huntingtin-interacting protein Hip-1 and a novel partner Hippi, Nat. Cell Biol. 4 (2002) 95–105, https://doi.org/10.1038/NCB735.

[10] D. Chen, J. Zhang, M. Li, E.R. Rayburn, H. Wang, R. Zhang, RYBP stabilizes p53 by modulating MDM2, EMBO Rep. 10 (2009) 166–172, https://doi.org/10.1038/EMBOR.2008.231.

[11] S. Fereres, R. Simón, A. Mohd-Sarip, C.P. Verrijzer, A. Busturia, dRYBP counteracts chromatin-dependent activation and repression of transcription, PLoS One 9 (2014), https://doi.org/10.1371/JOURNAL.PONE.0113255.
[12] R. Arrigoni, S.L. Alam, J.A. Wamstad, V.J. Bardwell, W.I. Sundquist, N. Schreiber-Agus, The Polycomb-associated protein Rybp is a ubiquitin binding protein, FEBS Lett. 580 (2006) 6233–6241, https://doi.org/10.1016/J.FEBSLET.2006.10.027.
[13] J. Zhao, M. Wang, L. Chang, J. Yu, A. Song, C. Liu, W. Huang, T. Zhang, X. Wu, X. Shen, B. Zhu, G. Li, RYBP/YAF2-PRC1 complexes and histone H1-dependent chromatin compaction mediate propagation of H2AK119ub1 during cell division, Nat. Cell Biol. 22 (2020) 439–452, https://doi.org/10.1038/S41556-020-0484-1.
[14] S. Schlisio, T. Halperin, M. Vidal, J.R. Nevins, Interaction of YY1 with E2Fs, mediated by RYBP, provides a mechanism for specificity of E2F function, EMBO J. 21 (2002) 5775–5786, https://doi.org/10.1093/EMBOJ/CDF577.
[15] J.L. Neira, M. Román-Trufero, L.M. Contreras, J. Prieto, G. Singh, F.N. Barrera, M. L. Renart, M. Vidal, The transcriptional repressor RYBP is a natively unfolded protein which folds upon binding to DNA, Biochemistry. 48 (2009) 1348–1360, https://doi.org/10.1021/BI801933C.
[16] R.B. Berlow, H.J. Dyson, P.E. Wright, Expanding the paradigm: intrinsically disordered proteins and allosteric regulation, J. Mol. Biol. 430 (2018) 2309–2320, https://doi.org/10.1016/J.JMB.2018.04.003.
[17] H. Xie, S. Vucetic, L.M. Iakoucheva, C.J. Oldfield, A.K. Dunker, V.N. Uversky, Z. Obradovic, Functional anthology of intrinsic disorder. 1. Biological processes and functions of proteins with long disordered regions, J. Proteome Res. 6 (2007) 1882–1898, https://doi.org/10.1021/PR060392U.
[18] M.M. Babu, R. van der Lee, N.S. de Groot, J. Gsponer, Intrinsically disordered proteins: regulation and disease, Curr. Opin. Struct. Biol. 21 (2011) 432–440, https://doi.org/10.1016/J.SBI.2011.03.011.
[19] J. Gsponer, M.E. Futschik, S.A. Teichmann, M.M. Babu, Tight regulation of unstructured proteins: from transcript synthesis to protein degradation, Science. 322 (2008) 1365–1368, https://doi.org/10.1126/SCIENCE.1163581.
[20] J.L. Neira, A. Jiménez-Alesanco, B. Rizzuti, A. Velazquez-Campoy, The nuclear localization sequence of the epigenetic factor RYBP binds to human importin α3, Biochim. Biophys. Acta, Proteins Proteomics 1869 (2021), https://doi.org/10.1016/J.BBAPAP.2021.140670.
[21] S.L. Alam, J. Sun, M. Payne, B.D. Welch, B.K. Blake, D.R. Davis, H.H. Meyer, S. D. Emr, W.I. Sundquist, Ubiquitin interactions of NZF zinc fingers, EMBO J. 23 (2004) 1411–1421, https://doi.org/10.1038/SJ.EMBOJ.7600114.
[22] M.A.M. Ali, H. Strickfaden, B.L. Lee, L. Spyracopoulos, M.J. Hendzel, RYBP is a K63-ubiquitin-chain-binding protein that inhibits homologous recombination repair, Cell Rep. 22 (2018) 383–395, https://doi.org/10.1016/J.CELREP.2017.12.047.
[23] W. Wang, J. Cheng, J.J. Qin, S. Voruganti, S. Nag, J. Fan, Q. Gao, R. Zhang, RYBP expression is associated with better survival of patients with hepatocellular carcinoma (HCC) and responsiveness to chemotherapy of HCC cells in vitro and in vivo, Oncotarget. 5 (2014) 11567–11582, https://doi.org/10.18632/ONCOTARGET.2598.
[24] D.V. Maybee, A.M. Psaras, T.A. Brooks, M.A.M. Ali, RYBP sensitizes cancer cells to PARP inhibitors by regulating ATM activity, Int. J. Mol. Sci. 23 (2022) 11764, https://doi.org/10.3390/IJMS231911764/S1.
[25] N.R. Jette, M. Kumar, S. Radhamani, G. Arthur, S. Goutam, S. Yip, M. Kolinsky, G. J. Williams, P. Bose, S.P. Lees-Miller, ATM-deficient cancers provide new opportunities for precision oncology, Cancers (Basel). 12 (2020) 687, https://doi.org/10.3390/CANCERS12030687.
[26] V. Zuco, V. Benedetti, F. Zunino, ATM- and ATR-mediated response to DNA damage induced by a novel camptothecin, ST1968, Cancer Lett. 292 (2010) 186–196, https://doi.org/10.1016/J.CANLET.2009.12.001.
[27] S.V. Kozlov, M.E. Graham, B. Jakob, F. Tobias, A.W. Kijas, M. Tanuji, P. Chen, P. J. Robinson, G. Taucher-Scholz, K. Suzuki, S. So, D. Chen, M.F. Lavin, Autophosphorylation and ATM activation, J. Biol. Chem. 286 (2011) 9119, https://doi.org/10.1074/JBC.M110.204065.
[28] N. McCabe, N.C. Turner, C.J. Lord, K. Kluzek, A. Białkowska, S. Swift, S. Giavara, M.J. O'Connor, A.N. Tutt, M.Z. Zdzienicka, G.C.M. Smith, A. Ashworth, Deficiency in the repair of DNA damage by homologous recombination and sensitivity to poly(ADP-ribose) polymerase inhibition, Cancer Res. 66 (2006) 8109–8115, https://doi.org/10.1158/0008-5472.CAN-06-0140.
[29] H.J. Park, J.S. Bae, K.M. Kim, Y.J. Moon, S.H. Park, S.H. Ha, U.K. Hussein, Z. Zhang, H.S. Park, B.H. Park, W.S. Moon, J.R. Kim, K.Y. Jang, The PARP inhibitor olaparib potentiates the effect of the DNA damaging agent doxorubicin in osteosarcoma, J. Exp. Clin. Cancer Res. 37 (2018) 107, https://doi.org/10.1186/S13046-018-0772-9.
[30] J. Murai, Y. Pommier, PARP trapping beyond homologous recombination and platinum sensitivity in cancers, Annu Rev Cancer Biol. 3 (2019) 131–150, https://doi.org/10.1146/ANNUREV-CANCERBIO-030518-055914.
[31] A. Min, S.A. Im, PARP inhibitors as therapeutics: beyond modulation of PARylation, Cancers (Basel). 12 (2020) 394, https://doi.org/10.3390/CANCERS12020394.
[32] Y. Matsuno, M. Hyodo, H. Fujimori, A. Shimizu, K.I. Yoshioka, Sensitization of cancer cells to radiation and topoisomerase I inhibitor Camptothecin using inhibitors of PARP and other signaling molecules, Cancers (Basel). 10 (2018) 364, https://doi.org/10.3390/CANCERS10100364.
[33] N.J. Curtin, C. Szabo, Therapeutic applications of PARP inhibitors: anticancer therapy and beyond, Mol. Asp. Med. 34 (2013) 1217–1256, https://doi.org/10.1016/J.MAM.2013.01.006.
[34] A.E. Yuzhalin, Citrullination in Cancer, Cancer Res. 79 (2019) 1274–1284, https://doi.org/10.1158/0008-5472.CAN-18-2797.
[35] N.S. Gudmann, N.U.B. Hansen, A.C.B. Jensen, M.A. Karsdal, A.S. Siebuhr, Biological relevance of citrullinations: diagnostic, prognostic and therapeutic options, Autoimmunity. 48 (2015) 73–79, https://doi.org/10.3109/08916934.2014.962024.
[36] A. Ishigami, N. Maruyama, Importance of research on peptidylarginine deiminase and citrullinated proteins in age-related disease, Geriatr Gerontol Int 10 Suppl 1 (2010), https://doi.org/10.1111/J.1447-0594.2010.00593.X.
[37] B. György, E. Tóth, E. Tarcsa, A. Falus, E.I. Buzás, Citrullination: a posttranslational modification in health and disease, Int. J. Biochem. Cell Biol. 38 (2006) 1662–1677, https://doi.org/10.1016/J.BIOCEL.2006.03.008.
[38] M. Guerrin, A. Ishigami, M.C. Méchin, R. Nachat, S. Valmary, M. Sebbag, M. Simon, T. Senshu, G., Serre, cDNA cloning, gene organization and expression analysis of human peptidylarginine deiminase type I, Biochem. J. 370 (2003) 174, https://doi.org/10.1042/BJ20020870.
[39] A. Ishigami, T. Ohsawa, H. Asaga, K. Akiyama, M. Kuramoto, N. Maruyama, Human peptidylarginine deiminase type II: molecular cloning, gene organization, and expression in human skin, Arch. Biochem. Biophys. 407 (2002) 25–31, https://doi.org/10.1016/S0003-9861(02)00516-7.
[40] T. Kanno, A. Kawada, J. Yamanouchi, C. Yosida-Noro, A. Yoshiki, M. Shiraiwa, M. Kusakabe, M. Manabe, T. Tezuka, H. Takahara, Human peptidylarginine deiminase type III: molecular cloning and nucleotide sequence of the cDNA, properties of the recombinant enzyme, and immunohistochemical localization in human skin, J. Investig. Dermatol. 115 (2000) 813–823, https://doi.org/10.1046/J.1523-1747.2000.00131.X.
[41] S. Chavanas, M.C. Méchin, H. Takahara, A. Kawada, R. Nachat, G. Serre, M. Simon, Comparative analysis of the mouse and human peptidylarginine deiminase gene clusters reveals highly conserved non-coding segments and a new human gene, PADI6, Gene. 330 (2004) 19–27, https://doi.org/10.1016/j.gene.2003.12.038.
[42] K. Nakashima, T. Hagiwara, A. Ishigami, S. Nagata, H. Asaga, M. Kuramotot, T. Senshu, M. Yamada, Molecular characterization of peptidylarginine deiminase in HL-60 cells induced by retinoic acid and 1α,25-dihydroxyvitamin D3, J. Biol. Chem. 274 (1999) 27786–27792, https://doi.org/10.1074/JBC.274.39.27786.
[43] S. Dong, T. Kanno, A. Yamaki, T. Kojima, M. Shiraiwa, A. Kawada, M.C. Méchin, S. Chavanas, G. Serre, M. Simon, H. Takahara, NF-Y and Sp1/Sp3 are involved in the transcriptional regulation of the peptidylarginine deiminase type III gene (PADI3) in human keratinocytes, Biochem. J. 397 (2006) 459, https://doi.org/10.1042/BJ20051939.
[44] S. Ying, S. Dong, A. Kawada, T. Kojima, S. Chavanas, M.C. Méchin, V. Adoue, G. Serre, M. Simon, H. Takahara, Transcriptional regulation of peptidylarginine deiminase expression in human keratinocytes, J. Dermatol. Sci. 53 (2009) 2–9, https://doi.org/10.1016/J.JDERMSCI.2008.09.009.
[45] D.J. Slade, S. Horibata, S.A. Coonrod, P.R. Thompson, A novel role for protein arginine deiminase 4 in pluripotency: the emerging role of citrullinated histone H1 in cellular programming, Bioessays. 36 (2014) 736–740, https://doi.org/10.1002/BIES.201400057.
[46] E. Witalison, P. Thompson, L. Hofseth, Protein arginine deiminases and associated citrullination: physiological functions and diseases associated with dysregulation, Curr. Drug Targets 16 (2015) 700–710, https://doi.org/10.2174/1389450116666150202160954.
[47] Y. Wang, R. Chen, Y. Gan, S. Ying, The roles of PAD2- and PAD4-mediated protein citrullination catalysis in cancers, Int. J. Cancer 148 (2021) 267–276, https://doi.org/10.1002/IJC.33205.
[48] C. Yang, Z.Z. Dong, J. Zhang, D. Teng, X. Luo, D. Li, Y. Zhou, Peptidylarginine deiminases 4 as a promising target in drug discovery, Eur. J. Med. Chem. 226 (2021), 113840, https://doi.org/10.1016/J.EJMECH.2021.113840.
[49] P. Li, D. Wang, H. Yao, P. Doret, G. Hao, Q. Shen, H. Qiu, X. Zhang, Y. Wang, G. Chen, Y. Wang, Coordination of PAD4 and HDAC2 in the regulation of p53-target gene expression, Oncogene. 29 (2010) 3153–3162, https://doi.org/10.1038/ONC.2010.51.
[50] P. Li, H. Yao, Z. Zhang, M. Li, Y. Luo, P.R. Thompson, D.S. Gilmour, Y. Wang, Regulation of p53 target gene expression by peptidylarginine deiminase 4, Mol. Cell. Biol. 28 (2008) 4745–4758, https://doi.org/10.1128/MCB.01747-07.
[51] J.L. Neira, S. Araujo-Abad, A. Cámara-Artigas, B. Rizzuti, O. Abian, A.M. Giudici, A. Velazquez-Campoy, C. de Juan Romero, Biochemical and biophysical characterization of PADI4 supports its involvement in cancer, Arch. Biochem. Biophys. 717 (2022), 109125, https://doi.org/10.1016/J.ABB.2022.109125.
[52] J.L. Neira, B. Rizzuti, O. Abián, S. Araujo-Abad, A. Velázquez-Campoy, C. de Juan Romero, Human enzyme PADI4 binds to the nuclear carrier importin α3, Cells. 11 (2022), https://doi.org/10.3390/CELLS11142166.
[53] J.L. Neira, B. Rizzuti, S. Araujo-Abad, O. Abian, M.E. Fárez-Vidal, A. Velazquez-Campoy, C. de Juan Romero, The armadillo-repeat domain of Plakophilin 1 binds to human enzyme PADI4, Biochim. Biophys. Acta, Proteins Proteomics 1871 (2023), https://doi.org/10.1016/J.BBAPAP.2022.140868.
[54] S. Araujo-Abad, J.L. Neira, B. Rizzuti, P. García-Morales, C. de Juan Romero, P. Santofimia-Castaño, J. Iovanna, Intrinsically disordered chromatin protein NUPR1 binds to the enzyme PADI4, J. Mol. Biol. 435 (2023), 168033, https://doi.org/10.1016/J.JMB.2023.168033.
[55] P. Santofimia-Castaño, B. Rizzuti, Á.L. Pey, P. Soubeyran, M. Vidal, R. Urrutia, J. L. Iovanna, J.L. Neira, Intrinsically disordered chromatin protein NUPR1 binds to the C-terminal region of polycomb RING1B, Proc. Natl. Acad. Sci. U. S. A. 114 (2017) E6332–E6341, https://doi.org/10.1073/PNAS.1619932114.
[56] C.E. Cano, T. Hamidi, M.J. Sandi, J.L. Iovanna, Nupr1: the Swiss-knife of cancer, J. Cell. Physiol. 226 (2011) 1439–1443, https://doi.org/10.1002/JCP.22324.
[57] Q. Jia, W. Zhou, W. Yao, F. Yang, S. Zhang, R. Singh, J. Chen, J.J. Chen, Y. Zhang, F. Wei, Y. Zhang, H. Jia, N. Wang, Downregulation of YAP-dependent Nupr1

promotes tumor-repopulating cell growth in soft matrices, Oncogenesis. 5 (2016), https://doi.org/10.1038/ONCSIS.2016.29.
[58] M.B. Lopez, M.N. Garcia, D. Grasso, J. Bintz, M.I. Molejon, G. Velez, G. Lomberk, J.L. Neira, R. Urrutia, J. Iovanna, Functional characterization of Nupr1L, a novel p53-regulated isoform of the high-mobility group (HMG)-related protumoral protein Nupr1, J. Cell. Physiol. 230 (2015) 2936–2950, https://doi.org/10.1002/JCP.25022.
[59] D. Clark, A. Mitra, R. Fillmore, W. Jiang, R. Samant, O. Fodstad, L. Shevde, NUPR1 interacts with p53, transcriptionally regulates p21 and rescues breast epithelial cells from doxorubicin-induced genotoxic stress, Curr. Cancer Drug Targets 8 (2008) 421–430, https://doi.org/10.2174/156800908785133196.
[60] S.C. Gill, P.H. von Hippel, Calculation of protein extinction coefficients from amino acid sequence data, Anal. Biochem. 182 (1989) 319–326, https://doi.org/10.1016/0003-2697(89)90602-7.
[61] M.P. Ventero, M. Fuentes-Baile, C. Quereda, E. Perez-Valeciano, C. Alenda, P. Garcia-Morales, D. Esposito, P. Dorado, V.M. Barbera, M. Saceda, Radiotherapy resistance acquisition in Glioblastoma. Role of SOCS1 and SOCS3, PLoS One. 14 (2019) doi:10.1371/JOURNAL.PONE.0212581.
[62] M. Fuentes-Baile, D. Bello-Gil, E. Pérez-Valenciano, J.M. Sanz, P. García-Morales, B. Maestro, M.P. Ventero, C. Alenda, V.M. Barberá, M. Saceda, CLytA-DAAO, free and immobilized in magnetic nanoparticles, induces cell death in human cancer cells, Biomolecules. 10 (2020), https://doi.org/10.3390/BIOM10020222.
[63] M. Fuentes-Baile, E. Pérez-Valenciano, P. García-Morales, C.J. de Romero, D. Bello-Gil, V.M. Barberá, Á. Rodríguez-Lescure, J.M. Sanz, C. Alenda, M. Saceda, CLytA-DAAO chimeric enzyme bound to magnetic nanoparticles. A new therapeutical approach for cancer patients? Int. J. Mol. Sci. 22 (2021) 1–24, https://doi.org/10.3390/IJMS22031477.
[64] J.L. Neira, F. Hornos, J. Bacarizo, A. Cámara-Artigás, J. Gómez, The monomeric species of the regulatory domain of tyrosine hydroxylase has a low conformational stability, Biochemistry. 55 (2016) 3418–3431, https://doi.org/10.1021/ACS.BIOCHEM.6B00135.
[65] B. Birdsall, R.W. King, M.R. Wheeler, C.A. Lewis, S.R. Goode, R.B. Dunlap, G.C. K. Roberts, Correction for light absorption in fluorescence studies of protein-ligand interactions, Anal. Biochem. 132 (1983) 353–361, https://doi.org/10.1016/0003-2697(83)90020-9.
[66] C.A. Royer, S.F. Scarlata, Fluorescence approaches to quantifying biomolecular interactions, Methods Enzymol. 450 (2008) 79–106, https://doi.org/10.1016/S0076-6879(08)03405-8.
[67] D. Beckett, Measurement and analysis of equilibrium binding titrations: a beginner's guide, Methods Enzymol. 488 (2011) 1–16, https://doi.org/10.1016/B978-0-12-381268-1.00001-X.
[68] M. Akdel, D.E.V. Pires, E.P. Pardo, J. Jänes, A.O. Zalevsky, B. Mészáros, P. Bryant, L.L. Good, R.A. Laskowski, G. Pozzati, A. Shenoy, W. Zhu, P. Kundrotas, V. R. Serra, C.H.M. Rodrigues, A.S. Dunham, D. Burke, N. Borkakoti, S. Velankar, A. Frost, J. Basquin, K. Lindorff-Larsen, A. Bateman, A.V. Kajava, A. Valencia, S. Ovchinnikov, J. Durairaj, D.B. Ascher, J.M. Thornton, N.E. Davey, A. Stein, A. Elofsson, T.I. Croll, P. Beltrao, A structural biology community assessment of AlphaFold2 applications, Nat. Struct. Mol. Biol. 29 (2022) 1056–1067, https://doi.org/10.1038/S41594-022-00849-W.
[69] J. Jumper, R. Evans, A. Pritzel, T. Green, M. Figurnov, O. Ronneberger, K. Tunyasuvunakool, R. Bates, A. Žídek, A. Potapenko, A. Bridgland, C. Meyer, S. A.A. Kohl, A.J. Ballard, A. Cowie, B. Romera-Paredes, S. Nikolov, R. Jain, J. Adler, T. Back, S. Petersen, D. Reiman, E. Clancy, M. Zielinski, M. Steinegger, M. Pacholska, T. Berghammer, S. Bodenstein, D. Silver, O. Vinyals, A.W. Senior, K. Kavukcuoglu, P. Kohli, D. Hassabis, Highly accurate protein structure prediction with AlphaFold, Nature. 596 (2021) 583–589, https://doi.org/10.1038/S41586-021-03819-2.
[70] R. Evans, M. O'Neill, A. Pritzel, N. Antropova, A. Senior, T. Green, A. Žídek, R. Bates, S. Blackwell, J. Yim, O. Ronneberger, S. Bodenstein, M. Zielinski, A. Bridgland, A. Potapenko, A. Cowie, K. Tunyasuvunakool, R. Jain, E. Clancy, P. Kohli, J. Jumper, D. Hassabis, Protein complex prediction with AlphaFold-Multimer, BioRxiv (2021), https://doi.org/10.1101/2021.10.04.463034, 2021.10.04.463034.
[71] R. Wang, A.B. Taylor, B.Z. Leal, L.V. Chadwell, U. Ilangovan, A.K. Robinson, V. Schirf, P.J. Hart, E.M. Lafer, B. Demeler, A.P. Hinck, D.G. McEwen, C.A. Kim, Polycomb group targeting through different binding partners of RING1B C-terminal domain, Structure. 18 (2010) 966–975, https://doi.org/10.1016/J.STR.2010.04.013.
[72] S. Mondal, P.R. Thompson, Protein arginine deiminases (PADs): biochemistry and chemical biology of protein citrullination, Acc. Chem. Res. 52 (2019) 818–832, https://doi.org/10.1021/ACS.ACCOUNTS.9B00024.
[73] D. Zhu, Y. Lu, Y. Wang, Y. Wang, PAD4 and its inhibitors in cancer progression and prognosis, Pharmaceutics. 14 (2022) 2414, https://doi.org/10.3390/PHARMACEUTICS14112414.
[74] J. Fuhrmann, K.W. Clancy, P.R. Thompson, Chemical biology of protein arginine modifications in epigenetic regulation, Chem. Rev. 115 (2015) 5413–5461, https://doi.org/10.1021/ACS.CHEMREV.5B00003.
[75] M. Mirdita, K. Schütze, Y. Moriwaki, L. Heo, S. Ovchinnikov, M. Steinegger, ColabFold: making protein folding accessible to all, Nat. Methods 19 (2022) 679–682, https://doi.org/10.1038/S41592-022-01488-1.
[76] D. Kozakov, D.R. Hall, B. Xia, K.A. Porter, D. Padhorny, C. Yueh, D. Beglov, S. Vajda, The ClusPro web server for protein–protein docking, Nature Protocols 12 (2) (2017) 255–278, doi:10.1038/nprot.2016.169.
[77] B. Rizzuti, Molecular simulations of proteins: from simplified physical interactions to complex biological phenomena, Biochimica et Biophysica Acta (BBA) Proteins and Proteomics 1870 (2022), 140757, https://doi.org/10.1016/J.BBAPAP.2022.140757.
[78] G. Weng, E. Wang, Z. Wang, H. Liu, F. Zhu, D. Li, T. Hou, HawkDock: a web server to predict and analyze the protein–protein complex based on computational docking and MM/GBSA, Nucleic Acids Res. 47 (2019) W322–W330, https://doi.org/10.1093/NAR/GKZ397.
[79] A. Onufriev, D. Bashford, D.A. Case, Exploring protein native states and large-scale conformational changes with a modified generalized born model, proteins: structure, Function, and Bioinformatics. 55 (2004) 383–394, https://doi.org/10.1002/PROT.20033.
[80] S. Matsuoka, G. Rotman, A. Ogawa, Y. Shiloh, K. Tamai, S.J. Elledge, Ataxia telangiectasia-mutated phosphorylates Chk2 in vivo and in vitro, Proc. Natl. Acad. Sci. U. S. A. 97 (2000) 10389, https://doi.org/10.1073/PNAS.190030497.
[81] K. Tan, X. Zhang, X. Cong, B. Huang, H. Chen, D. Chen, Tumor suppressor RYBP harbors three nuclear localization signals and its cytoplasm-located mutant exerts more potent anti-cancer activities than corresponding wild type, Cell. Signal. 29 (2017) 127–137, https://doi.org/10.1016/J.CELLSIG.2016.10.011.
[82] S. Zhan, T. Wang, W. Ge, J. Li, Multiple roles of ring 1 and YY1 binding protein in physiology and disease, J. Cell. Mol. Med. 22 (2018) 2054, https://doi.org/10.1111/JCMM.13503.
[83] C. Calés, L. Pavón, K. Starowicz, C. Pérez, M. Bravo, T. Ikawa, H. Koseki, M. Vidal, Role of Polycomb RYBP in maintaining the B-1-to-B-2 B-cell lineage switch in adult hematopoiesis, Mol. Cell. Biol. 36 (2015) 900–912, https://doi.org/10.1128/MCB.00869-15.
[84] Y. Wang, Y. Lyu, K. Tu, Q. Xu, Y. Yang, S. Salman, N. Le, H. Lu, C. Chen, Y. Zhu, R. Wang, Q. Liu, G.L. Semenza, Histone citrullination by PADI4 is required for HIF-dependent transcriptional responses to hypoxia and tumor vascularization, Sci. Adv. 7 (2021), https://doi.org/10.1126/SCIADV.ABE3771.
[85] H.D. Lewis, J. Liddle, J.E. Coote, S.J. Atkinson, M.D. Barker, B.D. Bax, K.L. Bicker, R.P. Bingham, M. Campbell, Y.H. Chen, C.W. Chung, P.D. Craggs, R.P. Davis, D. Eberhard, G. Joberty, K.E. Lind, K. Locke, C. Maller, K. Martinod, C. Patten, O. Polyakova, C.E. Rise, M. Rüdiger, R.J. Sheppard, D.J. Slade, P. Thomas, J. Thorpe, G. Yao, G. Drewes, D.D. Wagner, P.R. Thompson, R.K. Prinjha, D. M. Wilson, Inhibition of PAD4 activity is sufficient to disrupt mouse and human NET formation, Nat. Chem. Biol. 11 (2015) 191, https://doi.org/10.1038/NCHEMBIO.1735.
[86] M. Fuentes-baile, P. García-morales, E. Pérez-valenciano, M.P. Ventero, J. M. Sanz, C.J. de Romero, V.M. Barberá, C. Alenda, M. Saceda, Cell death mechanisms induced by CLytA-DAAO chimeric enzyme in human tumor cell lines, Int. J. Mol. Sci. 21 (2020) 8522, https://doi.org/10.3390/IJMS21228522.
[87] S. Kelly, N. Price, The use of circular dichroism in the investigation of protein structure and function, Curr. Protein Pept. Sci. 1 (2000) 349–384, https://doi.org/10.2174/1389203003381315.
[88] C. Perez-Iratxeta, M.A. Andrade-Navarro, K2D2: estimation of protein secondary structure from circular dichroism spectra, BMC Struct. Biol. 8 (2008) 1–5, https://doi.org/10.1186/1472-6807-8-25/TABLES/2.
[89] K. Arita, T. Shimizu, H. Hashimoto, Y. Hidaka, M. Yamada, M. Sato, Structural basis for histone N-terminal recognition by human peptidylarginine deiminase 4, Proc. Natl. Acad. Sci. U. S. A. 103 (2006) 5291–5296, https://doi.org/10.1073/PNAS.0509639103.
[90] P. Ulz, J. Belic, R. Graf, M. Auer, I. Lafer, K. Fischereder, G. Webersinke, K. Pummer, H. Augustin, M. Pichler, G. Hoefler, T. Bauernhofer, J.B. Geigl, E. Heitzer, M.R. Speicher, Whole-genome plasma sequencing reveals focal amplifications as a driving force in metastatic prostate cancer, Nat. Commun. 7 (2016), https://doi.org/10.1038/NCOMMS12008.
[91] A. Krohn, A. Seidel, L. Burkhardt, F. Bachmann, M. Mader, K. Grupp, T. Eichenauer, A. Becker, M. Adam, M. Graefen, H. Huland, S. Kurtz, S. Steurer, M.C. Tsourlakis, S. Minner, U. Michl, T. Schlomm, G. Sauter, R. Simon, H. Sirma, Recurrent deletion of 3p13 targets multiple tumour suppressor genes and defines a distinct subgroup of aggressive ERG fusion-positive prostate cancers, J. Pathol. 231 (2013) 130–141, https://doi.org/10.1002/PATH.4223.
[92] S.C. Stadler, C.T. Vincent, V.D. Fedorov, A. Patsialou, B.D. Cherrington, J. J. Wakshlag, S. Mohanan, B.M. Zee, X. Zhang, B.A. Garcia, J.S. Condeelis, A.M. C. Brown, S.A. Coonrod, C.D. Allis, Dysregulation of PAD4-mediated citrullination of nuclear GSK3β activates TGF-β signaling and induces epithelial-to-mesenchymal transition in breast cancer cells, Proc. Natl. Acad. Sci. U. S. A. 110 (2013) 11851–11856, https://doi.org/10.1073/PNAS.1308362110.
[93] D.V. Maybee, A.M. Psaras, T.A. Brooks, M.A.M. Ali, RYBP sensitizes cancer cells to PARP inhibitors by regulating ATM activity, Int. J. Mol. Sci. 23 (2022) 11764, https://doi.org/10.3390/IJMS231911764.
[94] A.A. Fatokun, V.L. Dawson, T.M. Dawson, Parthanatos: mitochondrial-linked mechanisms and therapeutic opportunities, Br. J. Pharmacol. 171 (2014) 2000–2016, https://doi.org/10.1111/BPH.12416.
[95] H. Farmer, H. McCabe, C.J. Lord, A.H.J. Tutt, D.A. Johnson, T.B. Richardson, M. Santarosa, K.J. Dillon, I. Hickson, C. Knights, N.M.B. Martin, S.P. Jackson, G.C. M. Smith, A. Ashworth, Targeting the DNA repair defect in BRCA mutant cells as a therapeutic strategy, Nature. 434 (2005) 917–921, https://doi.org/10.1038/nature03445.
[96] M. Yi, B. Dong, S. Qin, Q. Chu, K. Wu, S. Luo, Advances and perspectives of PARP inhibitors, Exp Hematol Oncol. 8 (2019), https://doi.org/10.1186/S40164-019-0154-9.
[97] N. Pu, W. Lou, J. Yu, PD-1 immunotherapy in pancreatic cancer: current status, J Pancreatol. 2 (2019) 6–10, https://doi.org/10.1097/JP9.0000000000000010.
[98] H. Yao, P. Li, B.J. Venters, S. Zheng, P.R. Thompson, B.F. Pugh, Y. Wang, Histone Arg modifications and p53 regulate the expression of OKL38, a mediator of

apoptosis, J. Biol. Chem. 283 (2008) 20060–20068, https://doi.org/10.1074/JBC.M802940200.
[99] E.R. Vossenaar, W.H. Robinson, Citrullination and autoimmune disease: 8th Bertine Koperberg meeting, Ann. Rheum. Dis. 64 (2005) 1513–1515, https://doi.org/10.1136/ARD.2005.045716.
[100] S. Zhan, T. Wang, W. Ge, J. Li, Multiple roles of ring 1 and YY1 binding protein in physiology and disease, J. Cell. Mol. Med. 22 (2018) 2046–2054, https://doi.org/10.1111/JCMM.13503.
[101] J. Zhao, M. Wang, L. Chang, J. Yu, A. Song, C. Liu, W. Huang, T. Zhang, X. Wu, X. Shen, B. Zhu, G. Li, RYBP/YAF2-PRC1 complexes and histone H1-dependent chromatin compaction mediate propagation of H2AK119ub1 during cell division, Nat. Cell Biol. 22 (2020) 439–452, https://doi.org/10.1038/S41556-020-0484-1.